



Research paper

Novel family of $[\text{RuCp}(\text{N},\text{N})(\text{P})]^+$ compounds with simultaneous anticancer and antibacterial activity: Biological evaluation and solution chemistry studies

Ricardo G. Teixeira^a, János P. Mészáros^{b,c}, Beatriz Matos^{d,e}, Leonor Côrte-Real^a, Cristina P.R. Xavier^{d,e}, Xavier Fontrodona^f, M. Helena Garcia^a, Isabel Romero^f, Gabriella Spengler^{c,g}, M. Helena Vasconcelos^{d,e,h}, Ana Isabel Tomaz^a, Éva A. Enyedy^{b,c}, Andreia Valente^{a,*}

^a Centro de Química Estrutural, Institute of Molecular Sciences, Departamento de Química e Bioquímica, Faculdade de Ciências, Universidade de Lisboa, Campo Grande, 1749-016, Lisboa, Portugal

^b Department of Molecular and Analytical Chemistry, Interdisciplinary Excellence Centre, University of Szeged, Dóm tér 7, H-6720, Szeged, Hungary

^c MTA-SZTE Lendület Functional Metal Complexes Research Group, University of Szeged, Dóm tér 7, H-6720, Szeged, Hungary

^d Instituto de Investigação e Inovação em Saúde (i3S), University of Porto, 4200-135, Porto, Portugal

^e Cancer Drug Resistance Group, Institute of Molecular Pathology and Immunology (IPATIMUP), University of Porto, 4200-135, Porto, Portugal

^f Departament de Química and Serveis Tècnics de Recerca, Universitat de Girona, C/ M. Aurèlia Campmany, 69, E-17003, Girona, Spain

^g Department of Medical Microbiology, Albert Szent-Györgyi Health Center and Albert Szent-Györgyi Medical School, University of Szeged, Semmelweis utca 6, 6725, Szeged, Hungary

^h Department of Biological Sciences, Faculty of Pharmacy of the University of Porto (FFUP), Porto, Portugal

ARTICLE INFO

Keywords:

Ruthenium-cyclopentadienyl

Anticancer

Antibacterial activity

MRSA

Solution studies

Anticancer activity

ABSTRACT

A family of ten novel ruthenium(II)-cyclopentadienyl organometallics of general formula $[\text{Ru}(\eta^5\text{-C}_5\text{H}_5)(\text{N},\text{N})(\text{PPh}_2(\text{C}_6\text{H}_4\text{COOR}))][\text{CF}_3\text{SO}_3]$ (**1–10**) in which (N,N) = 4,4'-R'-2,2'-bipyridyl (R = -H or -CH₂CH₂OH; R' = -H, -CH₃, -OCH₃, -CH₂OH, and -CH₂-biotin) was prepared from $[\text{Ru}(\eta^5\text{-C}_5\text{H}_5)(\text{PPh}_2(\text{C}_6\text{H}_4\text{COOH}))_2\text{Cl}]$. All compounds were fully characterized by means of several spectroscopic and analytical techniques, and the molecular structures of $[\text{Ru}(\eta^5\text{-C}_5\text{H}_5)(\text{PPh}_2(\text{C}_6\text{H}_4\text{COOH}))_2\text{Cl}]$, **1**, **3** and **4** have been additionally studied by single-crystal X-ray diffraction. The anticancer activity of all compounds was evaluated in sensitive and multidrug-resistant counterpart cell lines from human colorectal cancer (Colo 205 and Colo 320) and non-small cell lung cancer NSCLC (A549, NCI-H460 versus NCI-H460/R) as well. Notably, compounds **6** and **7** (R = CH₂CH₂OH and (N,N) = bipy or Me₂bipy, respectively) showed antiproliferative effect against both cell lines with high intrinsic selectivity towards cancer cells. The antibacterial activity of all compounds was also evaluated against both Gram negative and Gram positive strains, and some compounds in the series showed potent antibacterial activity against *Staphylococcus aureus* strains, including the methicillin-resistant MRSA strains.

Solution speciation studies revealed that the complexes bearing the $\text{PPh}_2(\text{C}_6\text{H}_4\text{COO}^-)$ ligand are neutral at physiological pH (7.4) in contrast with their ethylene glycol derivatives that have a permanent positive charge. While all compounds are lipophilic, the difference in the distribution coefficient for neutral and charged complexes is around one order of magnitude. Complexes **6** and **7** exhibited excellent biological activity and were selected for further studies. Spectrofluorometric methods were used to investigate their interaction with biomolecules such as human serum albumin (HSA) and calf thymus DNA (ct-DNA). For these complexes, binding site II of HSA is a possible binding pocket through non-covalent interactions. The release of ethidium from the DNA adduct by the charged complexes proves their interaction with DNA in contrast to the neutral ones.

In conclusion, Ru(II)-cyclopentadienyl complexes with 2,2'-bipyridyl-derivatives and an ethylene glycol moiety tethered to the phenylphosphane co-ligand are very promising from a therapeutic perspective, in particular complexes **6** and **7** that display remarkable antibacterial activity with a high anti-proliferative effect

* Corresponding author.

E-mail address: amvalente@ciencias.ulisboa.pt (A. Valente).

<https://doi.org/10.1016/j.ejmech.2023.115922>

Received 29 September 2023; Received in revised form 27 October 2023; Accepted 28 October 2023

Available online 31 October 2023

0223-5234/© 2023 The Authors. Published by Elsevier Masson SAS. This is an open access article under the CC BY-NC-ND license (<http://creativecommons.org/licenses/by-nc-nd/4.0/>).

against colon and non-small cell lung cancers, both clinically challenging neoplasias in need of effective solutions.

1. Introduction

The triumphs of platinum-based medications in clinical settings have urged researchers to explore the creation of new metallodrugs for cancer treatment. The potential of other metals in treating cancer has been receiving increased attention. In addition to platinum, several drugs based on ruthenium, copper, iron, and gallium have progressed through different phases of clinical trials in humans, demonstrating effectiveness in treating various forms of cancer [1]. Among the most promising candidates, ruthenium complexes have clearly emerged as front-runners by showing promising, often outstanding, results *in vitro* and *in vivo* against a wide range of human tumour cell lines, as well as a less toxic overall profile and (much desired) different mechanisms of action as compared to the clinically approved platinum-based drugs. Among them, imidazolium *trans*-[tetrachloro(dimethylsulfoxide)-(1*H*-imidazole)ruthenate(III)] (NAMI-A) and indazolium/sodium *trans*-[tetrachlorobis-(1*H*-indazole) ruthenate(III)] (KP1019/BOLD100®) are the only Ru(III)-based compounds that have entered clinical trials so far, together with the Ru(II) compound TLD-1433 ([Ru(4,4'-dimethyl-2,2'-bipyridine)₂-(2-(2',2'':5'',2''-terthiophene)-imidazo-[4,5-*f*][1,10]-phenanthroline)]Cl₂, Ruvidar®), all of them classical octahedral coordination complexes [2–5].

A distinct structural class of ruthenium compounds that has attracted the interest of many researchers are organoruthenium(II) complexes with a piano-stool geometry and bearing a ruthenium-arene scaffold (where arene is η^6 -benzene, η^6 -toluene, η^6 -*p*-cymene or derivatives) [6,

7] or a ruthenium-cyclopentadienyl core [8,9]. A common feature of all these Ru(II)-based compounds is the presence of at least one labile chlorido ligand, leading to the fact that the vast majority of these complexes exert their antiproliferative activity *via* ligand-exchange mechanisms, similarly to cisplatin [10], which can lead to excessive reactivity and chemical instability.

In the search for better stability under biologically relevant conditions, Marchetti and coworkers [11] have reported the conjugation of biotin to a ruthenium-*p*-cymene fragment by functionalization of the phosphane ligand (Fig. 1A). The introduction of anionic *O,O*-bidentate co-ligands into the organometallic scaffold (namely oxalato and curcuminato) resulted in structures with a superior stability profile in aqueous medium compared to the related analogue [RuCl₂(η^6 -*p*-cymene)(PPh₂R)] (R = PhCOOCH₂CH₂-biotin). Cytotoxic evaluation against HCT116, Colo 205, and SW620 colorectal cancer cells showed promising results in the low μ M concentration range.

Our research group has focused on the development of metallodrug candidates based on the Ru(II)-cyclopentadienyl ('RuCp') scaffold lacking labile ligands, namely involving the coordination of *N,N*-heteroaromatic and phosphane-based ligands in the remaining three-legged stool coordination positions [12,13]. In this approach, the Ru(II)-based drug candidate would behave as an active entity *per se* and would not require any activation like the organoruthenium(II) prodrug compounds mentioned above. Thus, we have been exploring the therapeutic potential of the general cationic structure [Ru(η^5 -C₅H₄R)(N,N)(P)]⁺ (where N,N =

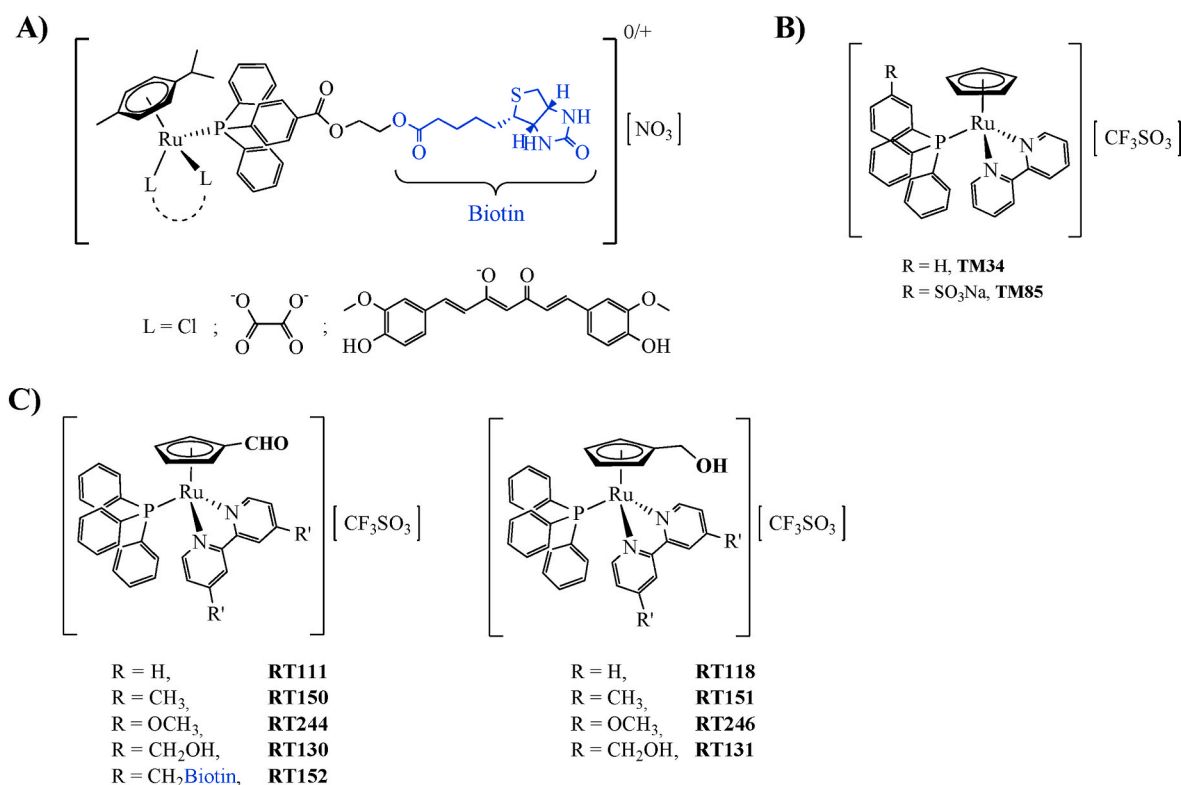


Fig. 1. Organoruthenium compounds with relevant anticancer activity. **A)** Active biotinylated 'Ru(arene)(LL)P' complexes (LL is either 2 chlorido monodentate ligands or a bidentate (*O,O*) ligand as pictured [11]; **B)** 'RuCp' Lead **TM34**, and its more water-soluble version **TM85** [16,18–20]; and **C)** [Ru(η^5 -C₅H₄R)(bipy-R') (P)]⁺ family with compounds **RT111**, **RT150**, **RT151**, **RT152**, **RT244** and **RT246** found to have: *i*) strong activity against cisplatin-resistant NSCLC cell lines, *ii*) inhibitory activity of MRP1 and P-gp efflux pumps, and *iii*) for **RT150** and **RT151** – high potential as collateral sensitivity inducers for cisplatin-resistant lung cancer cells [16,17]. In addition, the presence of an hydroxymethyl substituent seemed to be disadvantageous for the activity of the compounds in panel C, whether placed in the bipy ligand (in **RT130**) or in the cyclopentadienyl ring (in **RT118** and **RT131**).

2,2'-bipyridyl (bipy) derivatives; P = triphenylphosphane-based ligand; R = H, CH₃ [14,15], CHO [16,17], CH₂OH [16,17], CH₂-biotin [16]) due to its high stability, which allows for selective structural changes on its coordinating ligands towards structure-activity relationship analysis, aiming at solving unmet oncological challenges in the clinic. One of the lead structures (TM34, Fig. 1B) displayed extraordinary anticancer potential *in vitro*, but this compound exhibited poor aqueous solubility due to its highly lipophilic character [18,19]. As inadequate solubility and stability are considered major limitations for potential clinical application, we have used different strategies to address these limitations. In order to circumvent the aqueous solubility limitation of TM34, the triphenylphosphane co-ligand was replaced by a *meta*-monosulfonated derivative rendering [Ru(η^5 -C₅H₅)(bipy)(mTPPMS)][CF₃SO₃] (where mTPPMS = diphenylphosphane-benzene-3-sulfonate, TM85, Fig. 1B) [20]. This new compound possessed a markedly increased aqueous solubility with, however, a much significant decrease in anticancer activity, especially towards resistant and more aggressive cancer cell lines [20,21].

Further substitutions on the [Ru(η^5 -C₅H₄R)(N,N)(P)]⁺ scaffold led us to recently disclose a panel of 'RuCp' compounds with an unusual and valuable dual activity (Fig. 1C), namely high cytotoxicity and potent inhibition of ATP-Binding Cassette (ABC) efflux pumps. ABC pumps are known to be involved in multidrug resistance (MDR) mechanisms and are often overexpressed in resistant cancer cells [14,17,22]. Importantly, we also found that the introduction of methyl-, biotin-, and/or methoxy substituents at the 4 and 4'-position of the 2,2'-bipyridyl ligand was key to increase the overall cytotoxic effect against the cisplatin-resistant A549, NCI-H2228, and Calu-3 non-small cell lung cancer (NSCLC) cell lines [17]. In fact, these are the first 'RuCp'-based compounds reported with ability to sensitize NSCLC cells to the action of cisplatin, revealing these metallodrugs as new entities capable of modulating the performance of existing drugs used in the clinic.

In the search for better solubility in biologically relevant media (while maintaining the activity of the compounds) in this work we explored the introduction of an ethylene glycol moiety by functionalizing the phosphane co-ligand. For that, we have developed a family of 10 new 'RuCp' compounds bearing 2,2'-bipyridines with substituents at the 4,4'-positions, and an aryl-diphenylphosphane co-ligand derivatized either with a carboxylic acid group or an ethylene glycol-ester derivative.

In addition to the cytotoxic evaluation, characterization of the behaviour in solution is important to consider when assessing the biological evaluation of a new metallodrug candidate, and solution chemistry studies were also addressed in this work namely, stability, solubility, and lipophilicity as well as the robustness of the coordination set in the presence of competitive bioligands. Herein, we report our findings on this new family of ruthenium-cyclopentadienyl complexes with respect to all these aspects and disclose their high therapeutic value as prospective metallodrugs that can extend beyond cancer treatment application.

2. Results and discussion

2.1. Synthesis and characterization

A straightforward method used to isolate complexes with the general formula [Ru(η^5 -C₅H₅)(L)₂Cl] (where L = phosphane-based ligand) involves refluxing an ethanolic solution of hydrated ruthenium trichloride with an excess (typically 4 to 5 equivalents) of the tertiary phosphane and freshly distilled cyclopentadiene [23]. We used this route in our initial attempts to isolate a ruthenium cyclopentadienyl compound bearing the 4-(diphenylphosphino)benzoic acid ligand (PPh₂(C₆H₄COOH)). Alternatively, we refluxed a solution of [Ru(η^5 -C₅H₅)(PPh₃)₂Cl] with stoichiometric amounts of 4-(diphenylphosphino)benzoic acid in toluene, to promote the metathesis of the phosphane ligands at the complex (Scheme S1). By following this alternative procedure, we obtained the [Ru(η^5 -C₅H₅)(PPh₂(C₆H₄COOH))₂Cl] complex more efficiently by increasing

the reaction's yield up to 75% after work-up. Further reaction of [Ru(η^5 -C₅H₅)(PPh₂(C₆H₄COOH))₂Cl] with a series of 2,2'-bipyridine derivatives (bipy-R) in the presence of silver triflate as chloride abstractor, allowed to isolate five new cationic compounds with general formula [Ru(η^5 -C₅H₅)(bipy-R)(PPh₂(C₆H₄COOH))][CF₃SO₃], where bipy-R = 2,2'-bipyridyl (1), 4,4'-dimethyl-2,2'-bipyridyl (2), 4,4'-dimethoxy-2,2'-bipyridyl (3), 4,4'-bis(hydroxymethyl)-2,2'-bipyridyl (4) and 4,4'-dibiotin ester-2,2'-bipyridyl (5). Lastly, we functionalized the phosphane co-ligand in each complex 1–5 with an ethylene glycol moiety by activating the carboxylic acid group with *N*-(3-dimethylaminopropyl)-*N'*-ethylcarbodiimide hydrochloride (EDC•Cl) in a one-step procedure (Scheme S2). This DMAP-catalyzed reaction allowed the synthesis of five new compounds of general formula [Ru(η^5 -C₅H₅)(bipy-R)(PPh₂(C₆H₄COOCH₂CH₂OH))][CF₃SO₃] (where bipy-R = 2,2'-bipyridyl (6), 4,4'-dimethyl-2,2'-bipyridyl (7), 4,4'-dimethoxy-2,2'-bipyridyl (8), 4,4'-bis(hydroxymethyl)-2,2'-bipyridyl (9) and 4,4'-dibiotin ester-2,2'-bipyridyl (10) – Fig. 2, right) in moderate yield. The structure of all compounds was confirmed by several analytical and spectroscopic techniques including electrospray ionization mass spectrometry (ESI-MS), multinuclear NMR, FTIR and UVVisible (UVVis). The purity of all compounds was evaluated by elemental analysis. Single crystals of four compounds (namely [Ru(η^5 -C₅H₅)(PPh₂(C₆H₄COOH))₂Cl], 1, 3, and 4) were successfully obtained and studied in the solid state by X-ray crystallography, corroborating the structure proposed.

As expected, solid state FTIR spectra (in KBr pellets) of the new ruthenium-cyclopentadienyl complexes 1–10, presented bands for the ν_{C-H} stretching vibration in the range 3100–3050 cm⁻¹, and bands for the $\nu_{C=C}$ stretching ranging from 1430 to 1440 cm⁻¹ due to the phosphane, cyclopentadienyl and 2,2'-bipyridyl moieties. Moreover, the characteristic bands between 1260 and 1280 cm⁻¹ assigned to the asymmetric SO₃ stretching mode ν_{SO_3} of triflate were observed in the spectrum of all compounds, corroborating the presence of this counterion in the solid state, and thus their cationic nature. The presence of the carbonyl group was also detected in both sets of compounds through the appearance of the respective characteristic bands for aromatic $\nu_{C=O}$ ranging from 1690 cm⁻¹ to 1715 cm⁻¹. In the FTIR spectra of the set 6–10 the $\nu_{C=O}$ band shifted to a higher frequency (18–20 cm⁻¹ on average) providing evidence of the successful esterification of the carboxylic acid with ethylene glycol.

All resonances observed in the ¹H, ¹³C{¹H} and ³¹P{¹H} NMR spectra (Fig. S1–S11 in SI) were assigned based on the information obtained from 2D NMR experiments (COSY, HMQC and HMBC) and from coupling constants associated with the resonance signal. Overall, the ¹H NMR spectra of compounds 1–10 display a sharp singlet assigned to the cyclopentadienyl protons in the typical range for monocationic ruthenium(II)-cyclopentadienyl compounds (5.00 ppm < δ < 4.80 ppm) along with a set of multiplets in the aromatic region ascribed to the aryl-diphenylphosphane protons (δ 7.00–8.00 ppm). Compared to the precursor complex [Ru(η^5 -C₅H₅)(PPh₂(C₆H₄COOH))₂Cl], cyclopentadienyl resonances are observed downfield in the spectrum of each complex 1–10, as a consequence of the chloride abstraction and introduction of the *N,N*-bidentate derivative, as reported for related analogues [22,24]. As expected by the formation of the Ru(II) cationic species, σ -coordination of the 2,2'-bipyridyl derivatives causes a shift on the resonance signals associated with the protons of the cyclopentadienyl (Δ (C₅H₅ protons) ~ 0.8 ppm) and the 2,2'-bipyridyl co-ligands (e.g., Δ (H6 protons) ~ 0.8 ppm and Δ (H3 protons) ~ -0.4 ppm) for all the compounds. The resonance of the acid proton of the carboxylic acid present in 1–5 was observed downfield as a broad and well resolved signal at δ ~13.20 ppm. Both the protons of the cyclopentadienyl moiety and the protons of the substituents of the 2,2'-bipyridyl ligands do not change their chemical shift after esterification with ethylene glycol, and were observed upfield at δ 2.38 ppm (methyl protons for 2 and 7), δ 3.89 ppm (methoxy protons for 3 and 8), δ 4.60 ppm (hydroxymethyl protons for 4 and 9) and δ 5.17 ppm (methylene protons in the di-biotin ester of 5 and 10). After esterification with ethylene glycol, an additional set of signals

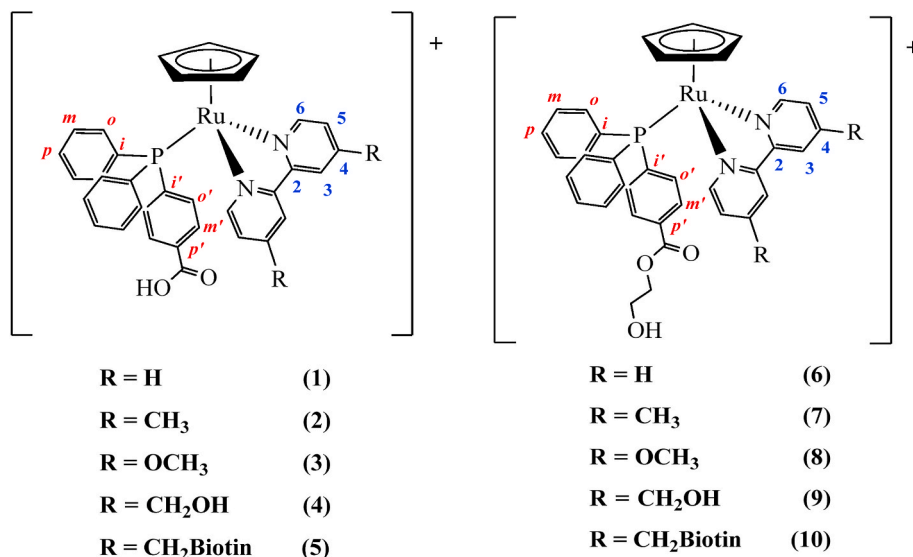


Fig. 2. The $[\text{RuCp}(\text{N,N})(\text{P})]^+$ family of compounds presented in this work: chemical structure of compounds 1–5 and compounds 6–10 (obtained from the former by derivatization of the phosphane) including the numbering scheme for spectral assignments. All compounds were isolated as CF_3SO_3^- salts.

is observed for compounds 6–10 related to the two methylene groups of the ethylene glycol moiety (δ 5.30–5.50 ppm). Data regarding ^{13}C $\{^1\text{H}\}$ -APT and $^{31}\text{P}\{^1\text{H}\}$ -NMR experiments are presented in detail in the experimental section, and are consistent with the effects discussed in the overall ^1H NMR analysis.

The electronic absorption spectra of compounds 1–10 were recorded in dichloromethane and DMSO (complex concentrations ranging from 10^{-4} M to 10^{-5} M) at room temperature. The electronic spectra of compounds 2 and 7 were selected as representative examples to illustrate the overall pattern of the absorption spectrum of each set (Fig. 3). A detailed description of the optical data (molar absorption coefficient values and corresponding wavelength (ϵ and λ_{max}) for all observed bands) is summarized in Table S1. Intense absorption bands in the UV range (up to $\lambda \sim 320$ –330 nm in both solvents) are observed in all spectra, which are attributed to ligand-based $\pi\text{--}\pi^*$ transitions of the coordinated chromophores and corresponding transitions in the organometallic fragment $\{[\text{Ru}(\eta^5\text{-C}_5\text{H}_5)(\text{PPh}_2(\text{C}_6\text{H}_4\text{COOR}))]\}^+$, ($\text{R}=\text{H}$; $\text{CH}_2\text{CH}_2\text{OH}$). Two medium-intense bands are observed in the visible range (between $\lambda \sim 330$ –380 nm and $\lambda \sim 400$ –540 nm) alongside these high-energy transitions. These bands are tentatively assigned as metal-to-ligand charge transfer transitions (MLCT) based on their energy and molar absorbance as seen in the case of related compounds [14,17,25]. Solvatochromism studies with the complexes were performed to explore the effect in the spectrum of a more polar solvent (DMSO). Globally, spectra of all compounds are less resolved in DMSO, with broader transitions centred at around $\lambda \sim 370$ –380 nm and showing evidence of a red-shift in these transitions with increasing polarity of the solvent. Together with a value of $\epsilon \sim 10^4 \text{ M}^{-1}\text{cm}^{-1}$, this confirms the CT nature of the mentioned bands.

2.2. Crystal structures of $[\text{Ru}(\eta^5\text{-C}_5\text{H}_5)(\text{PPh}_2(\text{C}_6\text{H}_4\text{COOH}))_2\text{Cl}]$, 1, 3 and 4

Single crystals suitable for X-ray diffraction studies of $[\text{Ru}(\eta^5\text{-C}_5\text{H}_5)(\text{PPh}_2(\text{C}_6\text{H}_4\text{COOH}))_2\text{Cl}]$ were grown from acetone, whereas single crystals of 1, 3 and 4 were isolated from slow diffusion of *n*-hexane into a solution of dichloromethane (1 and 3) or tetrahydrofuran (4). Figs. 4 and 5 show the ORTEP diagrams of the molecular structures for $[\text{Ru}(\eta^5\text{-C}_5\text{H}_5)(\text{PPh}_2(\text{C}_6\text{H}_4\text{COOH}))_2\text{Cl}]$ and compounds 1, 3 and 4, respectively. Selected bond distances and angles are included in the corresponding captions, while the main crystallographic data is summarized in the SI

section (Figs. S12 and S13).

Compounds $[\text{Ru}(\eta^5\text{-C}_5\text{H}_5)(\text{PPh}_2(\text{C}_6\text{H}_4\text{COOH}))_2\text{Cl}]$ and 1 crystallize in the monoclinic system, space groups $\text{P}2_1/\text{n}$ and $\text{P}2_1/\text{c}$, respectively; whereas 3 and 4 crystallize in the triclinic system, space group $\text{P}-1$. For 1, 3 and 4 the unit cell shows two enantiomers in the racemic crystals, like previously reported cyclopentadienyl ruthenium complexes [16]. The structures display the pseudo-octahedral piano-stool geometry around the ruthenium ions as expected, with the η^5 -cyclopentadienyl rings exhibiting a π -bonded coordination mode. The remaining three coordination sites are occupied in $[\text{Ru}(\eta^5\text{-C}_5\text{H}_5)(\text{PPh}_2(\text{C}_6\text{H}_4\text{COOH}))_2\text{Cl}]$ by a chlorido and two $\text{PPh}_2(\text{C}_6\text{H}_4\text{COOH})$ ligands, and in 1, 3, and 4 by a $\text{PPh}_2(\text{C}_6\text{H}_4\text{COOH})$ and a bidentate bipyridyl ligand. In the case of 3 and 4 the bipyridyl ligand contains two $-\text{OCH}_3$ and $-\text{CH}_2\text{OH}$ substituents, respectively. The distances between the ruthenium centers and the cyclopentadienyl centroids are in the range 1.829–1.844 Å, as it is the case with other similar compounds [17,26]. The same is true for Ru–P (2.292(15)–2.315(12) Å) and Ru–N (2.075(4)–2.099(5) Å) bond distances. It is noteworthy to point out the Ru–N bond distances in compounds 1, 3 and 4: in general, these distances are slightly shorter in 1 (containing the bipyridyl ligand) than in complexes 3 and 4 (with substituted bipyridyl ligands) (see caption of Fig. 5). This result is probably due to the electron donor character of $-\text{OCH}_3$ and $-\text{CH}_2\text{OH}$ substituents on the bipyridyl rings.

Values found for angles between the donors around the Ru cation are similar to those of other cyclopentadienyl compounds [17,26], with a larger P–Ru–P angle in comparison with P–Ru–Cl in $[\text{Ru}(\eta^5\text{-C}_5\text{H}_5)(\text{PPh}_2(\text{C}_6\text{H}_4\text{COOH}))_2\text{Cl}]$ probably due to steric hindrance of the phenyl substituents in the former. For 1, 3 and 4, the value of the N–Ru–N angles is indicative of the geometric restrictions of the bipyridyl ligands. On the other hand, for compound $[\text{Ru}(\eta^5\text{-C}_5\text{H}_5)(\text{PPh}_2(\text{C}_6\text{H}_4\text{COOH}))_2\text{Cl}]$, intramolecular hydrogen bonds are formed between the chlorido ligand and two hydrogen atoms of the $(\text{PPh}_2(\text{C}_6\text{H}_4\text{COOH}))$ ligands ($\text{H}19\text{--Cl}7 = 2.643$ Å and $\text{H}51\text{--Cl}7 = 2.991$ Å (Fig. S12A); additional strong intermolecular hydrogen bonds are observed between $-\text{COOH}$ substituents on the phosphane ligands of neighbouring molecules, determining the packing of this compound (Fig. S12B). In the case of 1, intermolecular hydrogen bonds are formed between one O atom of the CF_3SO_3^- anion and one H atom of the substituent $-\text{COOH}$ ($\text{H}17\text{--O}3\text{R} = 1.825$ Å (Fig. S13A). For compounds 3 and 4, two intermolecular bonds are observed between O atoms of CF_3SO_3^- anion and H atoms of the bipy ($\text{H}31\text{--O}4\text{S} = 2.553$ Å for 3, and $\text{H}38\text{--O}2\text{R} = 2.655$ Å for 4), and between

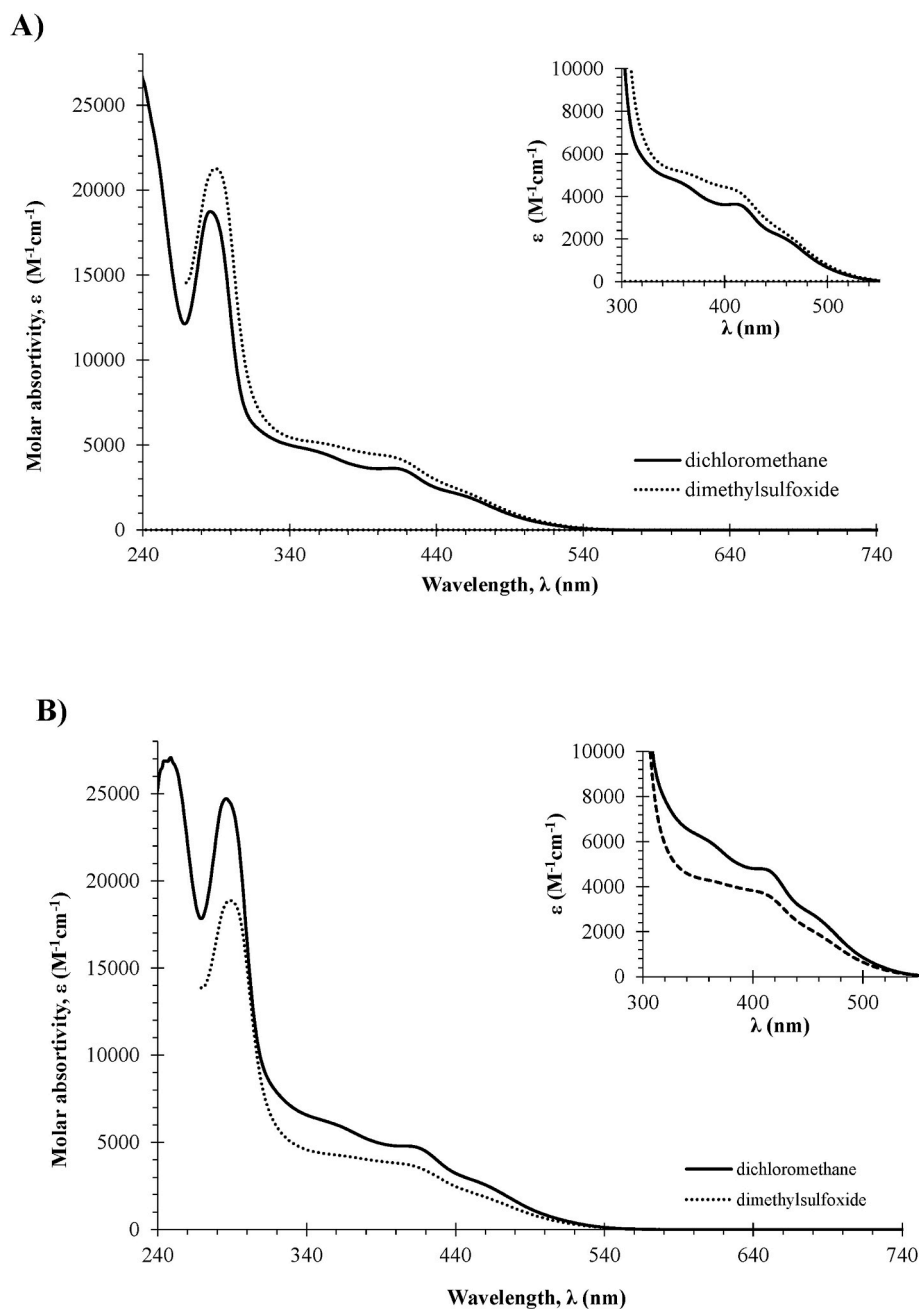


Fig. 3. Electronic absorption spectra of compounds **2** (A) and **7** (B) in dichloromethane (full line) and DMSO (dashed line) (see Table S1 for details.). Insets: Zoom into the range of lower intensity the spectrum - to evidence CT bands.

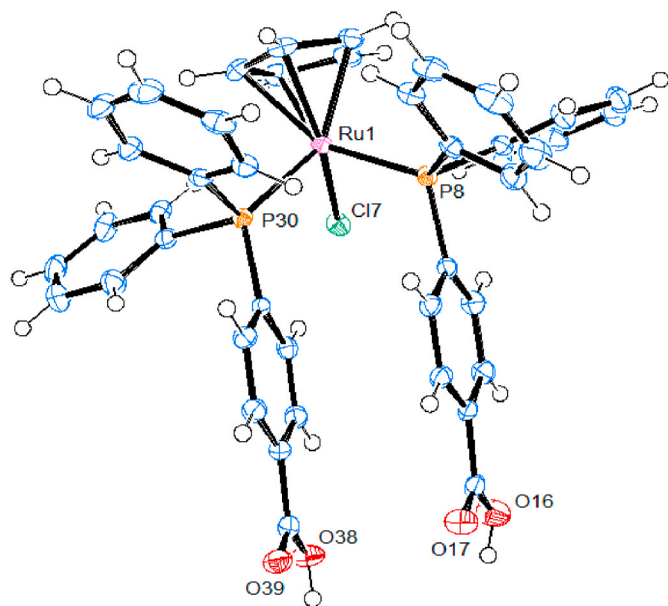
O atoms of the $-\text{OCH}_3$ or $-\text{CH}_2\text{OH}$ substituents on the bipy and H atoms of the phosphane ligands of neighbouring molecules ($\text{H28-O43} = 2.693 \text{ \AA}$ for **3**, and $\text{H12-O42} = 2.575 \text{ \AA}$ for **4**) (Figs. S13B and S13C).

2.3. Aqueous stability and lipophilicity of the complexes

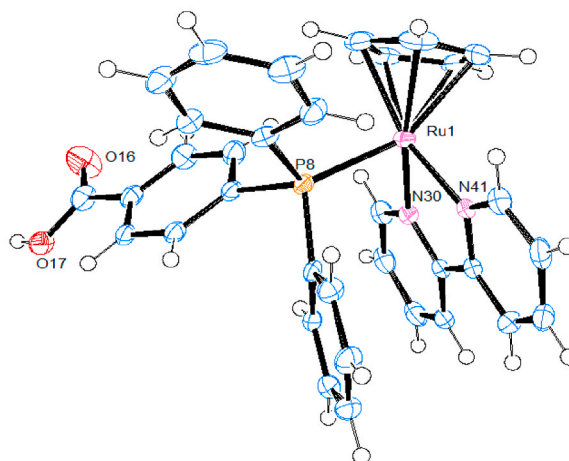
The aqueous stability of all compounds was studied prior to biological evaluation in order to infer about the robustness of the coordination sphere around the organometallic scaffold. DMSO is a strong coordinating solvent, particularly suited to solubilize most compounds and is frequently used as a co-solvent in biological studies. As such, we studied the stability in DMSO and in cell culture medium solution (DMEM and RPMI-1640) for a period of 24 h, at room temperature using UV-Vis spectrophotometry. Figs. S14–S17 gather these results and clearly show no significant spectral changes (absorbance variations below 10% after

24 h) under the various tested conditions, during the whole time period, confirming the extraordinary stability of the ligand set in either series of compounds. The stability of **1** and **6** in DMSO, and of **5** and **9** in buffer solution (30% DMSO- d_6 /70% phosphate buffer, pH = 7.4) was monitored by ^1H - and $^{31}\text{P}\{^1\text{H}\}$ -NMR spectroscopy as well. No changes were observed over 24 h in any spectra (Figs. S14 and S15) supporting the absence of structural changes on the compounds over time in these media.

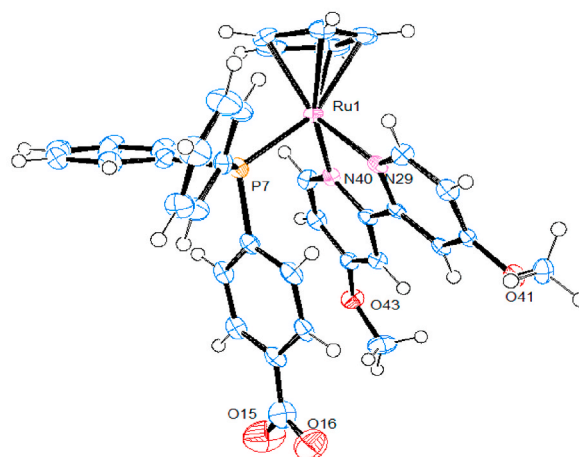
Complexes **1–5** incorporate the phosphane ligand with a carboxylic acid substituent that exhibits acid-base behaviour, affecting the charge of the whole complex according to the pH in solution. Thus, the UV-Vis spectra of complexes **1–5** show a pH-dependence (Fig. 6A), which can be attributed to the deprotonation of the coordinated 4-(diphenylphosphino)benzoic acid. By deconvolution of the recorded spectra at different pH values, we have determined the proton dissociation



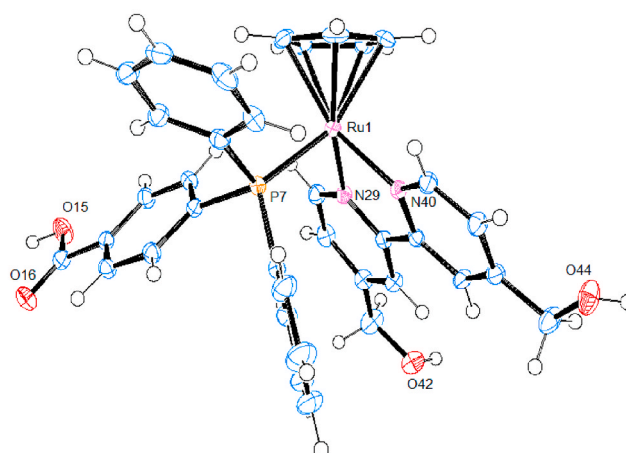
A)



B)



C)



(caption on next page)

Fig. 5. ORTEP plots and labeling schemes for the cations of compounds **1** (A), **3** (B) and **4** (C). Selected bond lengths (Å), angles (°) for **1**: Ru1–P8, 2.311(2); Ru1–N30, 2.086(4); Ru1–N41, 2.075(4); Ru1–Cp(centroid), 1.834; N30–Ru1–N41, 76.97(14); N30–Ru1–P8, 89.65(14); N41–Ru1–P8, 89.98(12); Cp(centroid)–Ru1–N41, 129.76; Cp(centroid)–Ru1–N30, 130.73; Cp(centroid)–Ru1–P8, 124.61; for **3**: Ru1–P7, 2.3068(16); Ru1–N29, 2.099(5); Ru1–N40, 2.096(5); Ru1–Cp(centroid), 1.836; N40–Ru1–N29, 76.07(18); N40–Ru1–P7, 90.63(14); N29–Ru1–P7, 89.09(13); Cp(centroid)–Ru1–N29, 130.81; Cp(centroid)–Ru1–N40, 129.20; Cp(centroid)–Ru1–P7, 125.47; for **4**: Ru1–P7, 2.2928(15); Ru1–N29, 2.099(2); Ru1–N40, 2.076(2); Ru1–Cp(centroid), 1.829; N40–Ru1–N29, 76.38(9); N29–Ru1–P7, 94.35(6); N40–Ru1–P7, 91.54(6); Cp(centroid)–Ru1–N29, 129.71; Cp(centroid)–Ru1–N40, 127.86; Cp(centroid)–Ru1–P7, 123.31.

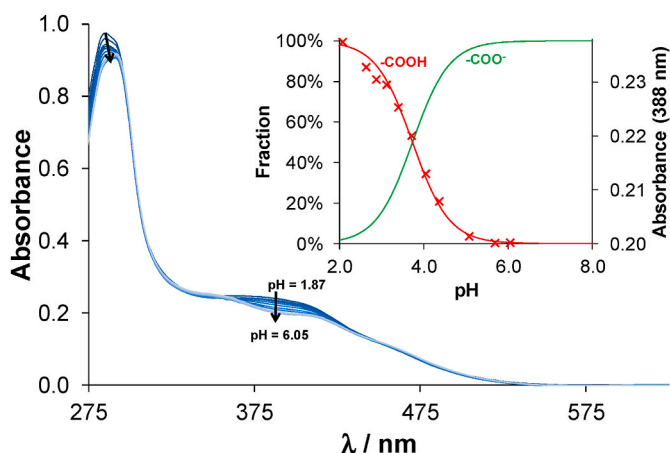


Fig. 6. UV–Vis spectra of complex **2** recorded in the pH range 1.87–6.05 in 30% (v/v) DMSO/H₂O solvent mixture. The inserted figure shows concentration distribution curves (using the obtained $pK_a = 3.99$) indicating the protonated (red; compound global charge +1) and deprotonated substituent (green; compound global charge: 0) together with the absorbance values at 388 nm as a function of pH for the same system. $c(\text{complex } 2) = 25.8 \mu\text{M}$, $I = 0.1 \text{ M (KCl)}$; $T = 25.0 \text{ }^\circ\text{C}$.

Table 1

IC₅₀ (μM) of all ruthenium compounds, doxorubicin, and cisplatin (positive controls) in human colorectal and lung cancer cell lines. The viability of cells was measured after 72 h incubation with increasing concentrations (0–100 μM) of each compound, measured with the MTT assay. n.d. = not determined.

PPh ₂ (C ₆ H ₄ R)	R at bipy	Compounds	IC ₅₀ (μM) ^a		
			Colo 205	Colo 320	A549
COOH	H	1	49.3 ± 2.1	n.d.	19.82 ± 0.48
	CH ₃	2	33.2 ± 1.1	n.d.	7.24 ± 0.58
	OCH ₃	3	54.52 ± 0.24	n.d.	13.49 ± 0.76
	CH ₂ OH	4	83.9 ± 3.2	n.d.	78.6 ± 4.1
	CH ₂ Biotin	5	8.06 ± 0.15	8.65 ± 0.45	29.18 ± 0.55
	H	6	30.41 ± 0.95	23.93 ± 0.25	3.83 ± 0.28
	CH ₃	7	4.76 ± 0.02	6.25 ± 0.12	0.69 ± 0.05
	OCH ₃	8	10.18 ± 0.10	11.94 ± 0.26	0.98 ± 0.09
	CH ₂ OH	9	44.06 ± 0.63	n.d.	35.8 ± 1.6
	CH ₂ Biotin	10	6.24 ± 0.17	7.44 ± 0.41	15.4 ± 1.1
COOCH ₂ CH ₂ OH		Doxorubicin	0.67 ± 0.03	1.29 ± 0.41	0.10 ± 0.02
		Cisplatin	3.33 ± 0.05	12.94 ± 0.73	9.5 ± 1.2

^a IC₅₀ values correspond to the mean ± standard error of the mean (S.E.M.) of at least three independent experiments.

be further studied regarding this feature. Interestingly, all compounds exhibit greater efficacy in the NSCLC line A549 compared to Colo 205 cells, except for the biotin-bearing compounds **5** and **10**.

We further selected the most potent complex **7** and the structurally simplest compound of the ethylene glycol series (**6**) that shows anti-MDR potential, together with their carboxylate analogues (**1** and **2**) to examine the tumour cell growth inhibitory activity in a sensitive non-small cell lung cancer cell line NCI-H460, and in its MDR counterpart cell line, NCI-H460/R, using the sulforhodamine B (SRB) assay (Table 2).

Our data demonstrated that complexes **6** and **7** presented a very low GI₅₀ concentration in the sensitive NCI-H460 cell line. Moreover, these two complexes were also more potent in the MDR counterpart cell line NCI-H460/R than the remaining studied compounds. However, compound **6** did not present a collateral sensitivity effect in the NCI-H460/R cell line, as had been previously verified in the Colo320 cell line. This might be justified by the different origin and genetic background of these colon and lung MDR cell lines. Interestingly, neither complex **6** nor **7** induced cytotoxic effects against the non-tumorigenic cell line MCF10A, at their GI₅₀ (concentrations that inhibits 50 % of cell growth) or at the double of the GI₅₀ concentrations found in the NCI-H460 cell line (Fig. S19).

Comparing these data with previous results for related compounds in several NSLC cell lines (A549, NCI-H2228, Calu-3 and NCI-H1975) and colorectal cells (cancerous RKO and SW480, and normal colon cell line NCM460) we can observe that the nature and position of the substituents at the different co-ligands highly influence the cytotoxicity of the compounds, being the groups introduced at the cyclopentadienyl ring those that affect the most the overall activity of the compounds [16,17,29]. Also, there is a general tendency of the complexes to be selective to cancer cells [29].

To further explore the mechanism of action of complexes **6** and **7**, we first evaluated whether the strong growth inhibitory effect observed for the NCI-H460 cells was due to an increase in cell death, using the Annexin V-FITC/PI labelling followed by flow cytometry analysis. Our results demonstrated that complex **7** significantly increased NCI-H460 cells death at 2 μM, when compared to the vehicle (Fig. 7).

Furthermore, the effect of the complexes **6** and **7** in the NCI-H460 cell cycle profile was assessed, using flow cytometry following propidium iodide (PI) staining. (Fig. 8).

Our results showed that complex **7** at 2 μM altered the cell cycle profile of the NCI-H460 cells, by causing a statistically significant increase in the % of cells in G1 phase of the cell cycle, together with a decrease the % of cells in S phase of the cell cycle, when compared to the

Table 2

GI₅₀ (Growth Inhibitory) concentrations of compounds **1**, **2**, **6** and **7** in the sensitive NCI-H460 and in its MDR counterpart NCI-H460/R non-small cell lung cancer cell line, determined by the SRB assay.

	GI ₅₀ (μM) ^a	
	NCI-H460	NCI-H460/R
1	7.6 ± 1.1	>100
2	3.40 ± 0.47	62.8 ± 5.7
6	0.92 ± 0.18	40.0 ± 3.9
7	0.43 ± 0.05	13.5 ± 1.5
Doxorubicin	0.021 ± 0.002	>100

^a GI₅₀ values correspond to the mean ± S.E.M. of at least three independent experiments.

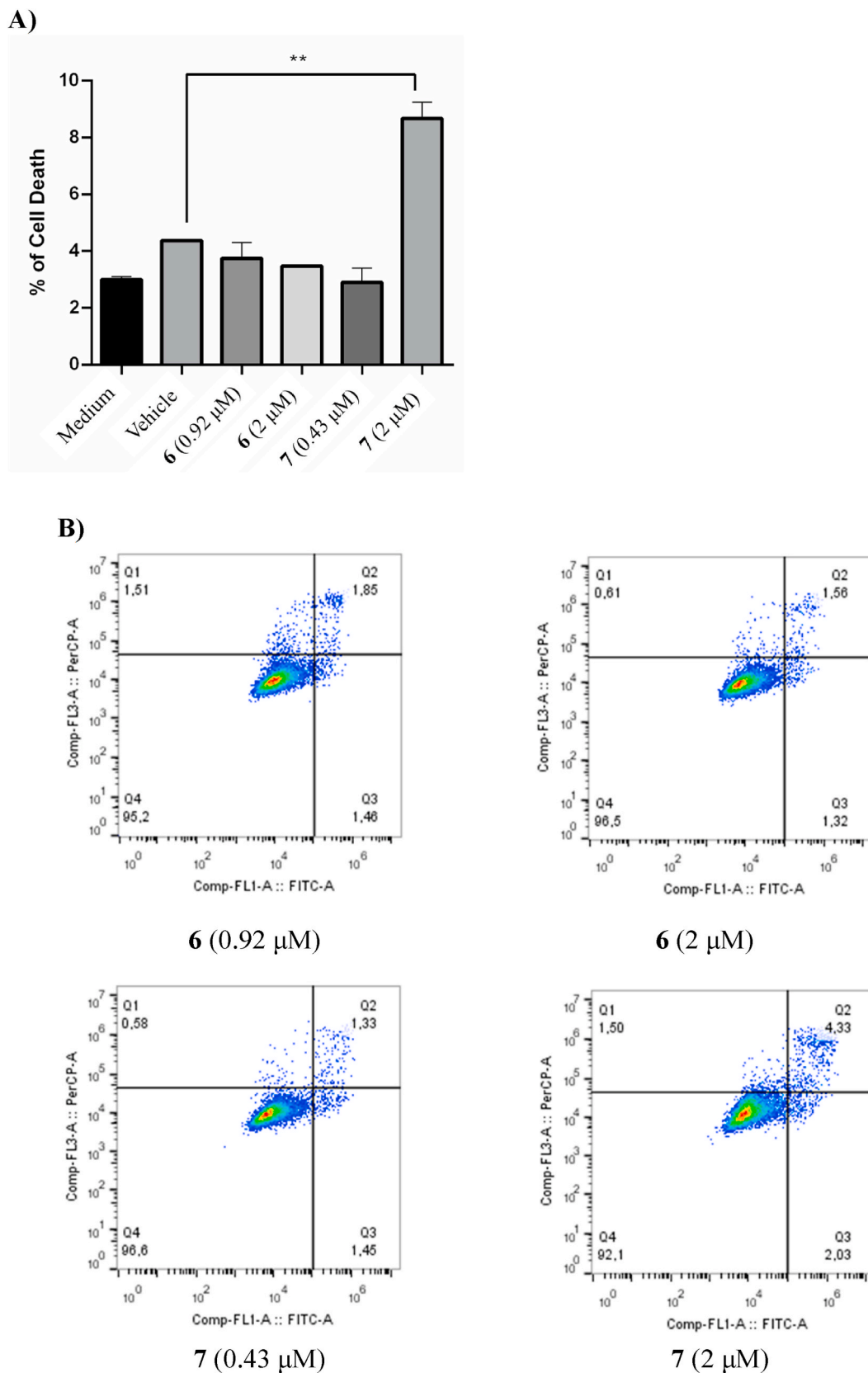
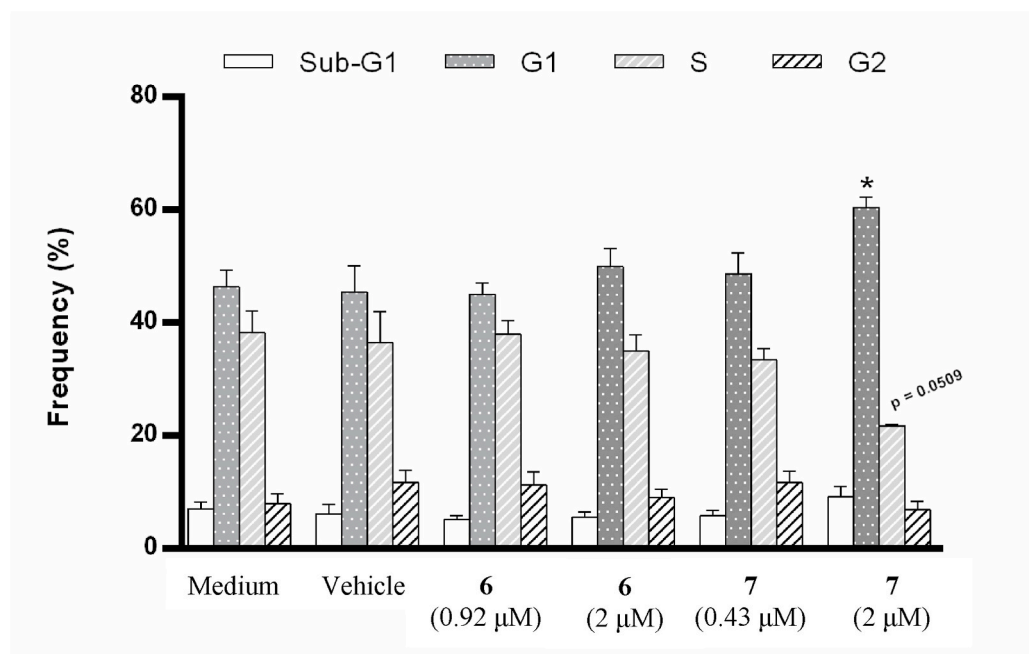
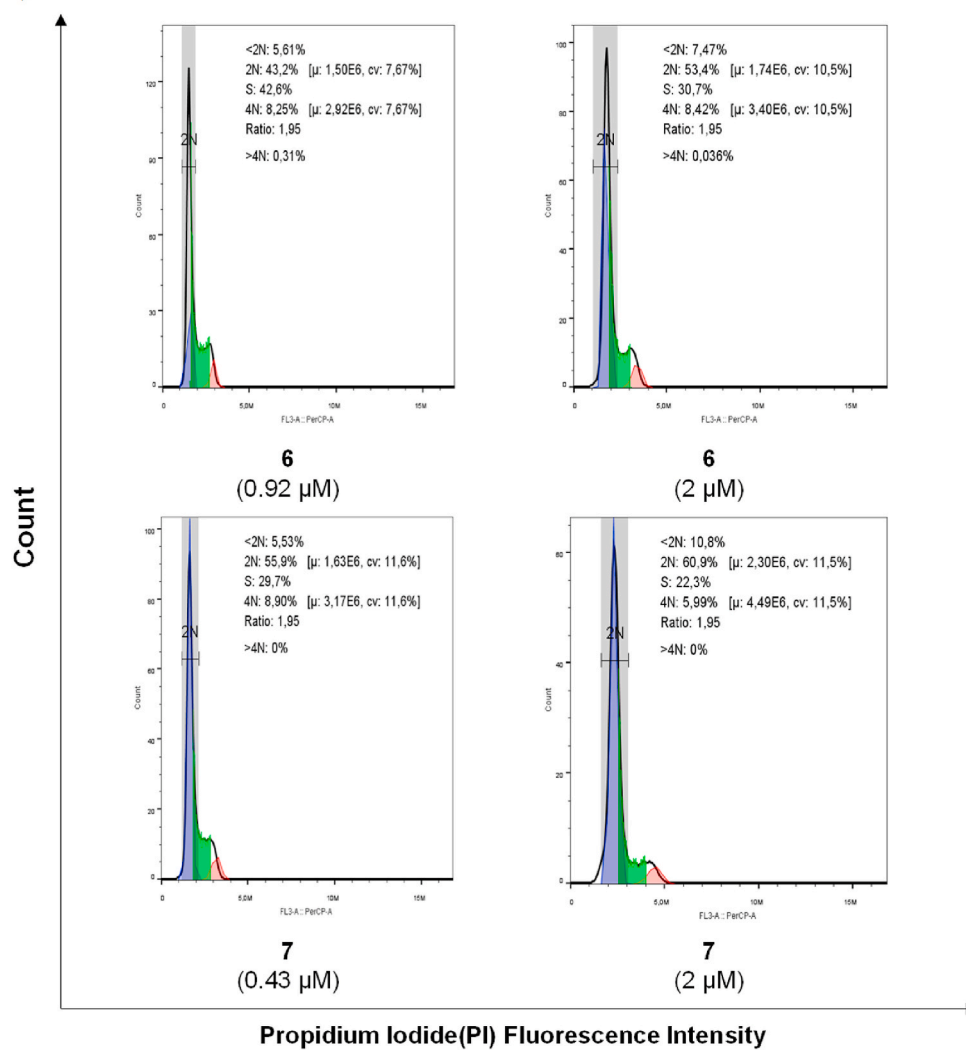


Fig. 7. Effect of the compounds **6** and **7** on the levels of NCI-H460 cells death, assessed by flow cytometry following Annexin V-FITC/PI staining. **A)** Cells were treated for 48 h with a) 0.92 μ M or 2 μ M of **6** and b) 0.43 μ M or 2 μ M of **7**. **B)** Representative dot plot cytograms showing % of cell death (Annexin V+ and/or PI+) and viable cells (Annexin V-PI-). The effect of the cells with the medium and with vehicle at the highest concentration tested in the drug treatments was also analysed, as controls (Fig. S20A). Results are the mean \pm SEM of at least three independent experiments. ** $p < 0.01$.



B)



(caption on next page)

Fig. 8. Effect of the compounds **6** and **7** on the cell cycle profile of NCI-H460 cells, assessed by flow cytometry following PI staining. **A)** Cells were treated for 48 h with i) 0.92 μM or 2 μM of **6** and ii) 0.43 μM or 2 μM of **7**. **B)** Representative cell cycle histograms, and frequency of cell cycle phases for each condition. The effect of the medium and the vehicle at the highest concentration tested in the drug treatments was also analysed (Fig. S20B). Results are the mean \pm SEM of at least three independent experiments. * $p < 0.05$.

vehicle. Taken together, our data demonstrated that complex **7** reduced NCI-H460 cell growth by impairing cell cycle profile and increasing cell death.

Complex **6**, which is structurally related with complex **7**, also decreased NCI-H460 cell growth, however without affecting the cell cycle profile or cell death, at the concentrations tested, suggesting other mechanisms of action for this complex. Further studies are required to understand the tumour cell growth inhibition effect of complex **6**.

The interest in metallodrugs in the quest for very competent therapeutics extends beyond cancer conditions onto other challenging medical issues like resistant bacterial infections. We addressed the therapeutic value of these compounds further, and screened them for their antibacterial effect.

2.5. Biological evaluation as antibacterial metallodrug candidates

Patients with cancer have weaker immune system and they are more sensitive to bacterial infections [30]. Multidrug-resistant bacterial strains are increasingly prevalent in hospitals, posing a severe threat to patients. Therefore, a cancer drug with efficacy against multidrug-resistant bacteria, in addition to individual disease treatment, would be highly beneficial. For this purpose, the antibacterial effect of all compounds was evaluated on Gram negative (*Escherichia coli* and *Klebsiella pneumoniae*) and on Gram positive bacteria (*S. aureus* ATCC 25923 and *S. aureus* MRSA ATCC 43300). Globally, based on the MIC values obtained, most of these metal complexes have strong antibacterial activity against *S. aureus* strains, including the methicillin-resistant MRSA strain (Table 3). According to the MIC values gathered these compounds could be sorted into three main categories: highly effective, medium effective, and with mild or no effect. Of note, complexes **1–10** showed no activity against the Gram negative strains – results not shown.

Complexes **6**, **7**, and **8** were highly effective on both the sensitive strain and on the MRSA strain, with MIC values ranging from 0.8 to 1.6 μM for MRSA. In fact, these three compounds showed a 10 to 20-fold improvement in MIC values against MRSA compared to reference antibiotics (see below). Complexes **9** and **10**, along with complexes **1**, **2**, and **3** belong to the group of compounds with medium activity against both strains. Complexes **4** and **5** exhibited the least efficacy against the sensitive strain with a MIC value of 50.0 and 25.0 μM , respectively). These derivatives had no effect on the MRSA strain, and hence are categorized as possessing ‘mild or no activity’. The difference observed between sensitive and methicillin-resistant *S. aureus* (MRSA) strains is due to the different membrane structure of resistant isolates (e.g., protein

composition of their membrane, differences in the type and number of efflux pumps, porins, membrane proteins) [31,32].

The trend was similar to the activity on A549 cells: the most active compounds were complexes **7** and **8**, while complex **4** was the least potent. Complexes **6–9** were more active in the resistant strain compared to the reference antibiotics, namely tetracycline (MIC >11.3 μM), gentamicin (MIC >10.5 μM) and ciprofloxacin (MIC >15.1), all based on our measurements in the same conditions, despite the lack of structural similarity. However, functionalization with biotin had no beneficial effects in their biological performance in this context.

Previous research has indicated that ruthenium compounds may hold promise in combating multidrug-resistant bacteria [1,33]. Yet, to the best of our knowledge, these are the first compounds based on $[\text{Ru}(\eta^5\text{-C}_5\text{H}_5)(\text{NN})(\text{P})]^+$ presenting such remarkable activity.

2.6. Transport and distribution in the system: interaction of the complexes with human serum albumin (HSA)

In the body, and regardless of its administration route, blood is the ultimate vehicle for the distribution and transport of a drug to target tissues and cells. The most abundant protein in the blood plasma is human serum albumin (HSA), a key player in the transport of various hydrophobic drugs, strongly affecting their pharmacokinetic properties [35]. It has two major drug binding sites as defined by Sudlow [35], namely site I (in subdomain IIA), which binds typically bulky heterocyclic anions with the charge situated in the center of the molecule, while neutral or negatively charged aromatic compounds are preferred to bind at site II (in subdomain IIIA) [36]. Moreover, the N-terminal residue in HSA can bind Cu(II) and Ni(II) metal ions (the so-called ATCUN motif), and solvent accessible amino acid side-chains provide various coordinative binding sites for metal complexes, e.g., Cys-34 and the surface-exposed His-128, His-247, His-510 and Met-298 [37]. The latter was described as potential binding sites for half-sandwich complexes with the general formula $[\text{Ru}(\text{arene})(\text{L})\text{Cl}]$ [37].

The interaction of complexes **1**, **2**, **6** and **7** with HSA was analysed using UV–Vis spectrophotometry and spectrofluorometry in phosphate buffer at pH 7.40. Over a 24 h period, no changes were observed in the UV–Vis spectra (at 1:1 HSA-to-metal complex ratio), indicating that albumin binding does not affect the metal coordination sphere, contrary to other organometallic arene complexes such as $[\text{Ru}(\text{arene})(\text{L})\text{Cl}]$ complexes. This is expected for stable complexes that can interact with the protein as a whole species, in an associative non-covalent binding process involving no ligand exchange like in the case of e.g. $[\text{Ru}(\text{p-cymene})(\text{picolinate})]$ [37].

If the interaction occurs through non-covalent binding (hydrogen bonding, van der Waals forces or hydrophobic interactions), drug binding site II is the most probable binding site for complexes under study (that are neutral or cationic), since neutral compounds are known to preferably bind there. However, binding was also tested in site I by following the emission intensity of Trp-214, which is located close to this binding pocket and can be excited selectively by 295 nm. In the case of a binding event at this site, the emission intensity of Trp-214 would be affected (most likely quenched). Preliminary tests proved no interaction up to 5 \times excess of complexes **6** and **7** with albumin (Fig. S21).

Dansylglycine (DG) is a site marker for site II, and its fluorescent intensity markedly increases upon binding to the protein. In the presence of a drug that preferably binds at the same site, DG can be displaced from the protein resulting in a concomitant decrease in the emission intensity [37]. The interaction of the chosen Ru complexes with HSA was investigated using DG displacement fluorescence studies. Samples

Table 3

MIC (μM) of all ruthenium compounds and positive controls (antibiotic drugs) against *S. aureus* ATCC 25923 and *S. aureus* MRSA 43300 strains.

	MIC (μM)		Activity
	<i>S. aureus</i> ATCC 25923	<i>S. aureus</i> MRSA ATCC 43300	
1	6.3	50.0	Medium efficacy (sensitive & MRSA)
2	3.1	12.5	
3	6.3	25.0	
4	50.0	>100	Weak activity/no effect
5	25.0	>100	
6	< 0.2	1.6	Highly effective (sensitive & MRSA)
7	< 0.2	0.8	
8	< 0.2	0.8	
9	1.6	6.3	Medium efficacy (sensitive & MRSA)
10	1.6	12.5	

contained HSA and DG at a fixed concentration (1:1 ratio, 5 μ M), and the metal complex was subsequently added in a 0.5–5 excess (Fig. 9).

Only a minor decrease in intensity change (<20%) was observable even in the presence of the 5-fold excess of the metal complexes (e.g., complex 6 in Fig. 9), indicating weaker interaction compared to the binding of DG in site II ($\log K' = 5.24$ [38]). Deconvolution of the steady-state emission spectra showed differences between the binding constants: $\log K' \sim 4.0$ for complex 6 and $\log K' = 3.1$ – 3.2 for complex 7. Under these conditions, the calculations indicate that 65.8% of DG is unbound to HSA in the absence of complex (equilibrium concentrations calculated from $\log K'(\text{HSA-DG}) = 5.24$) and this percentage increases to 69.7% and 66.4% at 5-fold excess of complex 6 and 7, respectively.

To clarify whether the spectral change was the result of dynamic quenching process or site-marker displacement by the metal complexes, fluorescence lifetime decays were also recorded. The time-correlated single photon counting (TCSPC) method enables the determination of the ratio of different emissive species present in the sample, their corresponding lifetimes, and provides clear evidence regarding the origin of the quenching that is observed. If the lifetime of the {HSA-DG} adduct changes upon addition of the complex, the quenching is considered as a dynamic quenching. Additionally, change in the α_i values (normalized amplitude of compound i , see below in Section “Instrumentation and methods”) is in connection with the increasing/decreasing molar fraction of the given species.

Data in Table S3 shows that the lifetime of {HSA-DG} adduct did not suffer any change, and the increasing α values of DG support the fact that the bound marker is liberated after the addition of the metal complex, showing the competition between the marker and the metal complex. The carboxylate derivatives complex 1 and 2 caused less changes in the α value of DG (Table S3), showing the weaker ability to compete with DG than the cationic complexes. Data shows that HSA has a slightly stronger preference for the binding of the cationic complexes over the neutral ones. Data obtained for complexes 1, 2 and 6, 7 are somewhat surprising when compared with the parent lead compound TM34, [Ru(Cp)(bipy)(PPh₃)]⁺, with no substitutions in the bipy or in the phosphane ligands that was evaluated in aqueous pH 7.4 media [18]. As for the tested complexes, no changes were observed by UV-Vis indicating that the whole parent complex is bound without any change in the coordination sphere. Binding of TM34 to HSA was found to be a fast process (≤ 30 min which suggests a “host-guest” type of interaction (in contrast with a covalent binding process that is typically slower to attain) as expected for a robust coordinatively saturated complex. The binding process occurred with the formation of a ground-state non-fluorescent 1:1 {complex-protein} adduct with adequate stability for TM34 to be transported by HSA in the blood stream. The presence of the

methyl substituent on the bipy co-ligand in the complex [Ru(Cp)(Me₂bipy)(PPh₃)]⁺ had little effect on its binding to HSA [39].

These results suggest that the functionalization on the phosphane co-ligand with a substituent/moiety that decreases the lipophilicity of the {Ru(Cp)(bipy)(P)} fragment is detrimental for the interaction with this protein. Thus, it can be hinted that the co-ligand PPh₃ (a very hydrophobic moiety) is playing a key role in the interaction in this family of {Ru(Cp)} complexes, with changes in its structure and/or lipophilicity having a marked impact on the ability for HSA binding.

2.7. Targets in the cell: interaction of the complexes with DNA (cell free media)

Regarding the subcellular distribution of the [Ru(Cp)(NN)(P)]⁺ complexes, previous studies indicate that they are present in the cell's nucleus in a very low percentage (<5%) indicating that DNA will not be the primary target for their action. Nevertheless, the interaction with DNA is also of great interest, since the platinum complexes currently used in clinical settings primary target DNA to exert their cytotoxic effect, and for several Ru complexes DNA is known to be involved in their action despite not being the primary target. Due to the lack of significant differences in the binding of complexes to HSA between those containing bipy and its dimethylated analogue, only complexes 1 and 6 were further studied for calf thymus DNA (ct-DNA) interaction. The interaction was studied by spectrofluorometry using ethidium bromide (EB) as a probe for the binding. Ethidium is a planar cation that can intercalate between DNA bases. Since its fluorescent intensity increases upon binding, this makes it an ideal marker for binding studies, and results are summarized in Fig. 10.

Marker displacement studies were performed at fixed (ct-DNA-base pair):EB = 2:1 ratio and metal complexes ratio, i.e., (metal complex)-to-(ct-DNA-base pair) ratio were varied between 0.5 and 5. A considerable decrease in the fluorescence intensity of the {ctDNA-EB} adduct with concomitant concentration increase of complex 6 (positively charged) is clear in Fig. 10A, supporting a binding interaction. In contrast with the considerable spectral changes in the presence of the complex 6, a minor decrease in the emission intensity was visible for complex 1. Upon deconvoluting the spectra, the ratio of free EB and the DNA-intercalated ethidium can be calculated, and results are collected in Fig. 10B. At a 5-fold excess of the metal complex, the amount ethidium released from the {ethidium-DNA} adduct is 15.4% for complex 6 and 2.1% for complex 1.

The mode of interaction is not clarified. Nevertheless, intercalation is hardly likely due to the structural features required for an intercalator that do not comply with the shape of the complex. Binding in the major or minor grooves can cause distortion in the structure of ct-DNA, which can result in the release of ethidium. It is possible that the {metal complex-ct-DNA} adduct formed may be stabilized by the electrostatic attraction of the negatively charged backbone of ct-DNA and the permanent positive charge of complex 6.

3. Conclusions

Continuing our studies on the relationship between structure, properties and activity with the organometallic Ru(II)-cyclopentadienyl scaffold, we designed and prepared a new family of structurally related compounds incorporating 4-(diphenylphosphino)benzoic acid and 2,2'-bipyridine derivatives as ligands, and examined the effect of functionalizing the phosphane co-ligand with ethylene glycol to yield more water-soluble compounds. All newly synthesized compounds were comprehensively characterized in both solution and the solid state (in some cases, by single crystal X-ray diffraction).

In general, complexes containing an ethylene glycol moiety showed lower lipophilicity and increased aqueous solubility under physiological mimetic conditions. This is connected to their overall charge, as the carboxylic acid functional group in complexes 1–5 is deprotonated under physiological conditions (pH = 7.4) resulting in a charge-neutral

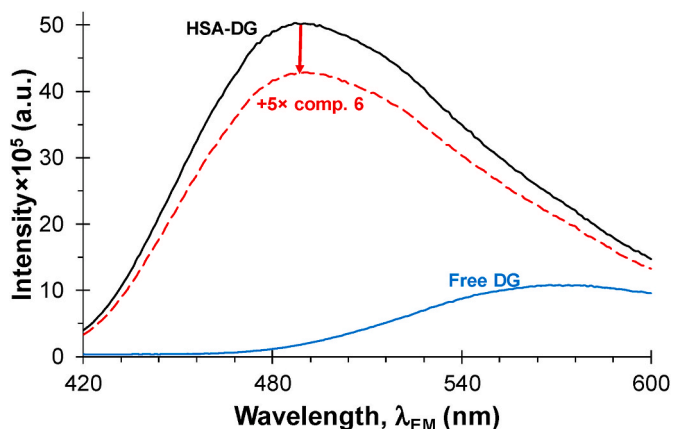


Fig. 9. Fluorescent spectra of free dansylglycine, HSA-DG (1:1) and HSA-DG-complex 6 (1:1:5) samples. $c(\text{HSA}) = c(\text{DG}) = 5 \mu\text{M}$, $c(\text{metal complex}) = 0$ – $25 \mu\text{M}$, $\lambda_{\text{ex}} = 335 \text{ nm}$, $\lambda_{\text{em}} = 420$ – 600 nm , pH = 7.40 (20 mM phosphate + 100 mM KCl), 2% (v/v) DMSO, T = 37 °C.

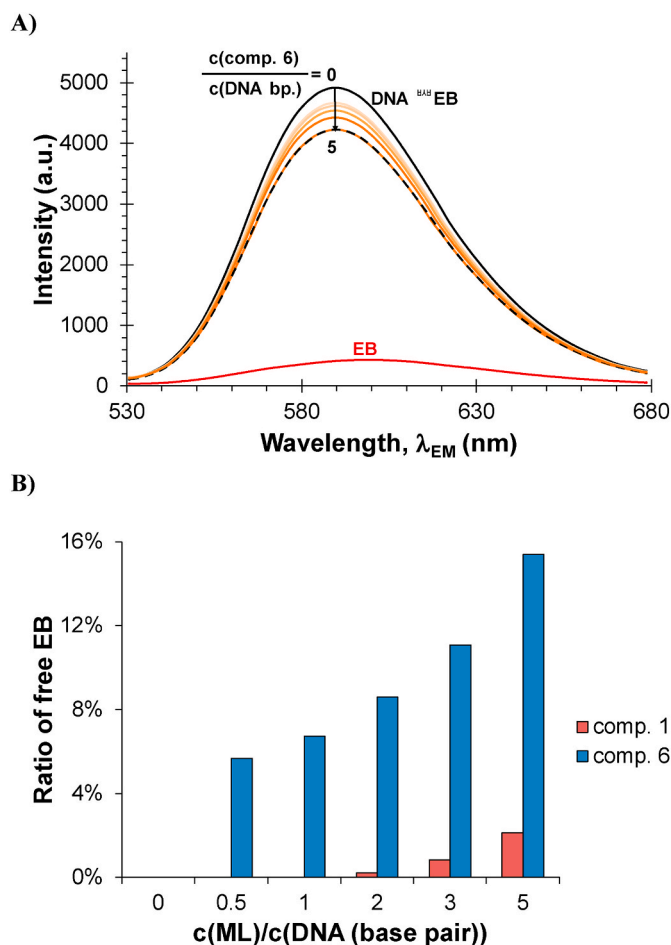


Fig. 10. A) Fluorescent spectra of free EB (full red line), {ct-DNA- E^+ } (2:1) (black full line, $c(\text{complex } 6) = 0$) and {DNA- E^+ -complex 6} (2:1:x) samples, where $x = 0; 0.5; 1; 2; 3; 5$ (yellow-orange-reddish colored light lines). B) Ratio of non-bound EB in the samples (ct-DNA-EB-metal complex) = (2:1:x) calculated based on the deconvolution of the recorded spectra; colour coding: dark red = complex 1, and blue = complex 6. $c(\text{EB}) = 5 \mu\text{M}$, $c(\text{ct-DNA (expressed as base pair)}) = 10 \mu\text{M}$, $c(\text{metal complex}) = 0\text{--}50 \mu\text{M}$, $\lambda_{ex} = 510 \text{ nm}$, $\lambda_{em} = 530\text{--}680 \text{ nm}$, $\text{pH} = 7.40$ (20 mM phosphate+4 mM KCl), 2 % DMSO, $T = 37^\circ\text{C}$.

species, while the ethylene glycol derivatives (complexes 6–10) possess a permanent positive charge. Overall, complexes 1–10 possess low thermodynamic solubility ($<400 \mu\text{M}$) in aqueous solution at $\text{pH } 7.4$. Complexes 6 and 7 (with a permanent localized cationic charge) were amongst the most soluble in water (at $\text{pH } 7.4$) while also displaying a good hydrophobic/hydrophilic balance ($\log D_{7.4} \sim +1.0$ and $+1.5$, respectively). The permanent charge displays stronger influence on the lipophilicity than on thermodynamic solubility, as complexes derivatized with ethylene glycol had in most of the cases (except biotin conjugates) higher hydrophilic character, even so these compounds still prefer the *n*-octanol phase.

Moreover, a different behaviour was also observed in the interaction with biomacromolecules. Binding to albumin is feasible through site II, as observed by competition experiments between the site marker dansylglycine and complexes 6 and 7. While it is likely that DNA is not the primary target of these complexes, exploring potential interactions with this molecule is meaningful for any metallodrug. While the cationic complex 6 was able to liberate the bound intercalator ethidium bromide from the {DNA-ethidium} adduct, its carboxylate and neutral counterpart complex 1 showed only a minimal interaction.

Concerning the biological assessment for lung and colon cancer models, the biotinylated complexes (5 and 10) and complex 7 were the most cytotoxic in Colo 205 cells. Complex 7 showed the highest

anticancer activity on Colo 205, Colo 320 and A549 cell lines. Complexes 6 and 7 were the most potent in inhibiting the growth of the NCI-H460 cell line, without causing cytotoxicity against the human non-tumorigenic cell line at the concentrations tested. Since compound 7 was the most potent, we further investigated its effect on cell death and cell cycle profile. We verified that complex 7 induced cell death and impaired the cell cycle profile of NCI-H460 cells, thus justifying the tumour cell growth inhibitory activity observed for 7.

The therapeutic potential of this family of compounds was also evaluated as prospective antibacterial drugs. In particular, the resistant MRSA strain is a growing common healthcare concern in hospital environments. Beyond the interest for all humans of new options to tackle resistant bacteria, the therapeutic potential of this family of compounds was also evaluated for their performance as potential antibacterial drugs. All compounds of this family underwent testing against both Gram positive and Gram negative strains. Contrary to their ineffectiveness against Gram negative strains (*E. coli* and *K. pneumoniae*), these compounds were found to be active to varying degrees against Gram positive *S. aureus* strains.

Our results show that compounds 6 and 7 have superior antibacterial activity against *S. aureus* ATCC 25923 and the resistant *S. aureus* MRSA 43300 strains, in the latter case far exceeding the activity of benchmark antibiotics such as tetracycline, gentamicin and ciprofloxacin.

In conclusion, from the panel of compounds presented in this work, two emerge as prospective metallodrugs that combine remarkable antibacterial activity with high anticancer activity against lung cancer and colon cancer, two cancer conditions still lacking good therapeutic options. To the best of our knowledge, these compounds are among the few examples of Ru complexes that show both strong anticancer and strong antibacterial activity.

4. Instrumentation and methods (experimental section)

4.1. Materials

All chemicals were purchased from commercial sources and used without further purification (unless otherwise stated).

4.2. General procedures

All reactions and purification of compounds were performed under nitrogen atmosphere using Schlenk techniques. All solvents used for the organometallic synthesis were distilled under nitrogen atmosphere before use, according to common literature methods, except for dichloromethane, *n*-hexane and tetrahydrofuran (used for synthesis and work-up) that were dried using an MBRAUN solvent purification system (MB SPS-800, M Braun Inertgas-Systeme GmbH, Garching, Germany). NMR spectra were recorded on a Bruker Avance 400 spectrometer at probe temperature (298 K) using commercially available deuterated acetone and dimethylsulfoxide. Chemical shifts (δ) are reported in parts per million (ppm) referenced to tetramethylsilane (δ 0.00 ppm) using the residual proton solvent peaks as internal standards. The multiplicity of the peaks is abbreviated as follows: s (singlet), d (doublet), t (triplet), m (multiplet), comp (complex). Coupling constants (J) are reported in Hertz (Hz). All assignments were attributed using COSY, HMBC, and HMQC bidimensional-NMR techniques. Infrared spectra were recorded on KBr pellets using a Mattson Satellite FT-IR spectrophotometer. Only considered relevant bands were cited in the text. Electronic spectra were recorded at room temperature on a Jasco V-660 spectrometer from solutions of 10^{-4} – 10^{-5} M in quartz cuvettes (1 cm optical path), under air and at room temperature. Elemental analyses were performed at *Laboratório de Análises*, at *Instituto Superior Técnico*, using a Fisons Instruments EA1108 system. ESI-MS data acquisition, integration and handling were performed using a PC with the software package EAGER-200 (Carlo Erba Instruments).

4.3. Synthesis of the ruthenium complexes

4.3.1. Synthesis of the precursor compound $[\text{Ru}(\eta^5\text{-C}_5\text{H}_5)(\text{PPh}_2(\text{C}_6\text{H}_4\text{COOH}))_2\text{Cl}]$

This compound was isolated by two different methods.

4.3.1.1. Method A. A portion of dry powdered molecular sieves was placed in a Schlenk, to which a stirred solution of $\text{RuCl}_3 \cdot x\text{H}_2\text{O}$ (0.407 g, 1.96 mmol) in ethanol (50 mL), 4-(diphenylphosphino)benzoic acid (1.501 g, 4.90 mmol) and freshly distilled cyclopentadiene (5 mL) were added. The dark brown mixture was stirred under reflux for 8 h until no more precipitation of the orange-yellowish compound was observed. Then, the mixture was cooled down overnight in the fridge (4 °C). The precipitate was filtered and washed nine times with acetone (30 mL) to extract the compound from the powdered molecular sieves. All fractions were collected in a round bottom flask and the solvent evaporated. The final residue was washed with water (20 mL x 2), cold ethanol (20 mL x 2) and a mixture of ethanol and light petroleum ether (50:50 (% v/v), 20 mL x 2) and then dried in vacuum overnight.

Yield: 60% (960 mg).

4.3.1.2. Method B. To a solution of $[\text{Ru}(\eta^5\text{-C}_5\text{H}_5)(\text{PPh}_3)_2\text{Cl}]$ (550 mg, 0.75 mmol) in 30 mL of toluene 4-(diphenylphosphino)benzoic acid (510 mg, 1.65 mmol) was added. The resulting mixture was vigorously stirred under reflux for 2.5 h. Over the course of the reaction the intended compound separates from the solution as a yellowish precipitate. The solid obtained was isolated from the reaction mixture by filtration (while hot) and then washed with diethyl ether (10 mL x 3) and dried in vacuum overnight.

Yield: 75% (416 mg).

^1H NMR $[(\text{CD}_3)_2\text{SO}, \text{Me}_4\text{Si}]$ δ (ppm): 12.97 (s br, 2H, COOH), 7.68 (d, 4H, $^3J_{\text{HH}} = 8$, Hm'), 7.33–7.18 (comp, 24H, Ho' + Ho + Hm + Hp), 4.12 (s, 5H, C₅H₅). APT- $^{13}\text{C}\{^1\text{H}\}$ NMR $[(\text{CD}_3)_2\text{SO}]$ δ (ppm): 166.9 (COOH), 143.2 (Co'), 137.6 (Cm'), 134.4, 133.1, 130.9 (Cp'), 129.3 (Cp), 128.31, 127.8, 81.5 (C₅H₅). $^{31}\text{P}\{^1\text{H}\}$ NMR $[(\text{CD}_3)_2\text{SO}]$ δ (ppm): 39.5 (s, PPh₂(C₆H₄COOH)). FTIR [KBr, cm⁻¹]: 3100–3049 (ν_{C-H} aromatic rings), 1692 (ν_{C=O}), 1481–1432 (ν_{C=C} aromatic rings), 1299 (ν_{C-O}). UV–Vis [DMSO, λ_{max}/nm (ε x 10³/M⁻¹cm⁻¹)]: 348 (3.67). Elemental analysis calc. for C₄₃H₃₅ClO₄P₂Ru (740.21 g mol⁻¹): C, 59.4; H, 4.10. Found: C, 59.5; H, 4.3. ESI-MS: [M – Cl] + calc. for [C₄₃H₃₅O₄P₂Ru]⁺: 779.11, found: 779.05 (25 %); [M-Cl-H + NCH₃]⁺ calc. for [C₄₅H₃₇NO₄P₂Ru]⁺: 819.12, found: 819.52 (100 %).

4.3.2. Syntheses of the complexes $[\text{Ru}(\eta^5\text{-C}_5\text{H}_5)(\text{bipy-R})(\text{PPh}_2(\text{C}_6\text{H}_4\text{COOH}))][\text{CF}_3\text{SO}_3]$ (1–5)

Complexes of general formula $[\text{Ru}(\eta^5\text{-C}_5\text{H}_5)(\text{bipy-R})(\text{PPh}_2(\text{C}_6\text{H}_4\text{COOH}))][\text{CF}_3\text{SO}_3]$ (1–5) were prepared from the parent neutral compound $[\text{Ru}(\eta^5\text{-C}_5\text{H}_5)(\text{PPh}_2(\text{C}_6\text{H}_4\text{COOH}))_2\text{Cl}]$ (150 mg, 0.18 mmol) by halide abstraction with silver trifluoromethanesulfonate (54 mg, 0.20 mmol) in degassed methanol (20 mL) and in the presence of a slight excess (1.2 equivalents) of 2,2'-bipyridine (for 1, 35 mg, 0.22 mmol), 4,4'-dimethyl-2,2'-bipyridine (for 2, 41 mg, 0.22 mmol), 4,4'-dimethoxy-2,2'-bipyridine (for 3, 47 mg, 0.22 mmol), 4,4'-hydroxymethyl-2,2'-bipyridine (for 4, 48 mg, 0.22 mmol) or 4,4'-dibiotinester-2,2'-bipyridine (for 5, 148 mg, 0.22 mmol) for 13–18 h at reflux under nitrogen atmosphere. After cooling to room temperature, filtering, and removing the solvent, the compounds were washed with *n*-hexane (3 x 10 mL) and recrystallized from slow diffusion of *n*-hexane into dichloromethane (1, 2, 3, and 5) or tetrahydrofuran (4), to give orange crystalline solids.

4.3.2.1. $[\text{Ru}(\eta^5\text{-C}_5\text{H}_5)(2,2'\text{-bipy})(\text{PPh}_2(\text{C}_6\text{H}_4\text{COOH}))][\text{CF}_3\text{SO}_3]$ (1). Yield: 62% (89 mg). Orange single crystals were obtained from slow diffusion of *n*-hexane into a dichloromethane solution.

^1H NMR $[(\text{CD}_3)_2\text{SO}, \text{Me}_4\text{Si}]$ δ (ppm): 13.21 (s br, 1H, COOH), 9.36 (d,

2H, $^3J_{\text{HH}} = 6$, H6), 8.19 (d, 2H, $^3J_{\text{HH}} = 8$, H3), 7.85 (t, 1H, $^3J_{\text{HH}} = 8$, H4), 7.76 (d, 2H, $^3J_{\text{HH}} = 8$, Hm'), 7.43 (t, 2H, $^3J_{\text{HH}} = 8$, Hp), 7.33 (t, 6H, Ho + H5), 7.01 (t, 5H, $^3J_{\text{HH}} = 8$, Hm), 6.94 (t, 2H, $^3J_{\text{HH}} = 8$, Ho'), 4.88 (s, 5H, C₅H₅). APT- $^{13}\text{C}\{^1\text{H}\}$ NMR $[(\text{CD}_3)_2\text{SO}]$ δ (ppm): 166.7 (COOH), 156.1 (C6), 155.2 (C2), 136.3 (d + s, $^1J_{\text{CP}} = 38$, C4 + C1'), 132.8 (d, $^2J_{\text{CP}} = 12$, C5), 132.4 (d, $^2J_{\text{CP}} = 12$, C3), 130.8 (d, $^1J_{\text{CP}} = 42$, C1), 130.3 (br, Cp), 128.9 (d, $^3J_{\text{CP}} = 10$, Cm'), 128.7 (d, $^3J_{\text{CP}} = 10$, Cm), 125.1 (C5), 123.5 (C3), 78.6 (d, $^2J_{\text{CP}} = 1$, C₅H₅). $^{31}\text{P}\{^1\text{H}\}$ NMR $[(\text{CD}_3)_2\text{SO}]$ δ (ppm): 52.3 (s, PPh₂(C₆H₄COOH)). FTIR [KBr, cm⁻¹]: 3105–3076 (ν_{C-H} aromatic rings), 1695 (ν_{C=O}), 1433 (ν_{C=C} aromatic rings), 1274 (ν_{CF₃SO₃} counterion). UV–Vis [DMSO, λ_{max}/nm (ε x 10³/M⁻¹cm⁻¹)]: 292 (19.50), 352 (sh), 422 (3.58), 486 (sh). UV–Vis [CH₂Cl₂, λ_{max}/nm (ε x 10³/M⁻¹cm⁻¹)]: 290 (18.39), 348 (sh), 418 (3.92), 492 (sh). Elemental analysis calc. for C₃₅H₂₈F₃N₂O₅PRuS (777.71 g mol⁻¹): C, 54.05; H, 3.63; N, 3.60; S, 4.12. Found: C, 54.1; H, 3.5; N, 3.6; S, 4.0. ESI-MS: [1-CF₃SO₃] + calc. for [C₃₄H₂₈N₂O₂PRu]⁺: 629.09, found: 629.03 (100 %).

4.3.2.2. $[\text{Ru}(\eta^5\text{-C}_5\text{H}_5)(4,4'\text{-CH}_3\text{-2,2'\text{-bipy}})(\text{PPh}_2(\text{C}_6\text{H}_4\text{COOH}))][\text{CF}_3\text{SO}_3]$ (2). Yield: 57% (85 mg).

^1H NMR $[(\text{CD}_3)_2\text{SO}, \text{Me}_4\text{Si}]$ δ (ppm): 13.19 (s br, 1H, COOH), 9.16 (d, 2H, $^3J_{\text{HH}} = 6$, H6), 8.01 (s, 2H, H3), 7.74 (d, 2H, $^3J_{\text{HH}} = 8$, Hm'), 7.45 (t, 2H, $^3J_{\text{HH}} = 8$, Hp), 7.37 (t, 4H, $^3J_{\text{HH}} = 8$, Ho), 7.18 (d, 2H, $^3J_{\text{HH}} = 8$, H5), 7.08 (t, 4H, $^3J_{\text{HH}} = 8$, Hm), 6.86 (t, 2H, $^3J_{\text{HH}} = 8$, Ho'), 4.82 (s, 5H, C₅H₅), 2.38 (s, 6H, CH₃). APT- $^{13}\text{C}\{^1\text{H}\}$ NMR $[(\text{CD}_3)_2\text{SO}]$ δ (ppm): 166.8 (COOH), 155.3 (br, C6), 154.9 (C2), 148.1 (C4), 136.3 (d, $^1J_{\text{CP}} = 38$, C1'), 133.1 (d, $^2J_{\text{CP}} = 12$, C5), 132.2 (d, $^2J_{\text{CP}} = 12$, C3), 131.6 (Cp'), 131.2 (d, $^1J_{\text{CP}} = 42$, C1), 130.3 (br, Cp), 128.9 (d, $^3J_{\text{CP}} = 10$, Cm'), 128.6 (d, $^3J_{\text{CP}} = 10$, Cm), 126.0 (C5), 123.9 (C3), 78.1 (d, $^2J_{\text{CP}} = 1$, C₅H₅), 20.3 (CH₃). $^{31}\text{P}\{^1\text{H}\}$ NMR $[(\text{CD}_3)_2\text{SO}]$ δ (ppm): 52.3 (s, PPh₂(C₆H₄COOH)). FTIR [KBr, cm⁻¹]: 3118–3047 (ν_{C-H} aromatic rings), 2980 (ν_{C-H} alkanes), 1699 (ν_{C=O}), 1423 (ν_{C=C} aromatic rings), 1276 (ν_{CF₃SO₃} counterion). UV–Vis [DMSO, λ_{max}/nm (ε x 10³/M⁻¹cm⁻¹)]: 292 (21.80), 368 (sh), 415 (sh), 470 (sh). UV–Vis [CH₂Cl₂, λ_{max}/nm (ε x 10³/M⁻¹cm⁻¹)]: 255 (sh), 291 (18.60), 364 (sh), 409 (3.79), 471 (sh). Elemental analysis calc. for C₃₇H₃₂F₃N₂O₅PRuS (805.76 g mol⁻¹): C, 55.15; H, 4.00; N, 3.48; S, 3.98. Found: C, 55.2; H, 4.2; N, 3.7; S, 4.0. ESI-MS: [2-CF₃SO₃] + calc. for [C₃₆H₃₂N₂O₂PRu]⁺: 657.12, found: 657.02 (100 %).

4.3.2.3. $[\text{Ru}(\eta^5\text{-C}_5\text{H}_5)(4,4'\text{-OCH}_3\text{-2,2'\text{-bipy}})(\text{PPh}_2(\text{C}_6\text{H}_4\text{COOH}))][\text{CF}_3\text{SO}_3]$ (3). Yield: 61% (94 mg). Orange single crystals were obtained from slow diffusion of *n*-hexane into a dichloromethane solution.

^1H NMR $[(\text{CD}_3)_2\text{SO}, \text{Me}_4\text{Si}]$ δ (ppm): 13.21 (s br, 1H, COOH), 9.05 (d, 2H, $^3J_{\text{HH}} = 6$, H6), 7.80 (d, 2H, $^3J_{\text{HH}} = 2$, H3), 7.75 (d, 2H, $^3J_{\text{HH}} = 8$, Hm'), 7.44 (t, 3H, $^3J_{\text{HH}} = 8$, Hp), 7.36 (t, 3H, $^3J_{\text{HH}} = 8$, Hp), 7.09 (t, 4H, $^3J_{\text{HH}} = 8$, Ho), 6.96 (d, 2H, $^3J_{\text{HH}} = 8$, H5), 6.92 (t, 2H, $^3J_{\text{HH}} = 8$, Hm), 4.77 (s, 5H, C₅H₅), 3.89 (s, 6H, OCH₃). APT- $^{13}\text{C}\{^1\text{H}\}$ NMR $[(\text{CD}_3)_2\text{SO}]$ δ (ppm): 167.3 (COOH), 166.3 (C4), 157.1 (C6), 157.0 (C2), 137.4 (d, $^1J_{\text{CP}} = 38$, C1'), 133.4 (d, $^2J_{\text{CP}} = 12$, C5), 132.8 (d, $^2J_{\text{CP}} = 12$, C3), 132.1 (Cp'), 131.9 (d, $^1J_{\text{CP}} = 42$, C1), 130.6 (br, Cp), 129.4 (d, $^3J_{\text{CP}} = 10$, Cm'), 129.1 (d, $^3J_{\text{CP}} = 10$, Cm), 112.9 (C5), 110.2 (C3), 77.9 (d, $^2J_{\text{CP}} = 2$, C₅H₅), 57.0 (-OCH₃). $^{31}\text{P}\{^1\text{H}\}$ NMR $[(\text{CD}_3)_2\text{SO}]$ δ (ppm): 52.9 (s, PPh₂(C₆H₄COOH)). FTIR [KBr, cm⁻¹]: 3095–3071 (ν_{C-H} aromatic rings), 2987–2946 (ν_{C-H} alkanes), 1715 (ν_{C=O}), 1435 (ν_{C=C} aromatic rings), 1268 (ν_{CF₃SO₃} counterion). UV–Vis [DMSO, λ_{max}/nm (ε x 10³/M⁻¹cm⁻¹)]: 289 (26.27), 371 (7.21), 412 (sh). UV–Vis [CH₂Cl₂, λ_{max}/nm (ε x 10³/M⁻¹cm⁻¹)]: 290 (26.10), 366 (6.91), 412 (sh). Elemental analysis calc. for C₃₇H₃₂F₃N₂O₇PRuS (837.76 g mol⁻¹): C, 53.05; H, 3.85; N, 3.34; S, 3.83. Found: C, 53.3; H, 4.0; N, 3.5; S, 4.0. ESI-MS: [3-CF₃SO₃] + calc. for [C₃₆H₃₂N₂O₄PRu]⁺: 689.11, found: 688.97 (100 %).

4.3.2.4. $[\text{Ru}(\eta^5\text{-C}_5\text{H}_5)(4,4'\text{-CH}_2\text{OH-2,2'\text{-bipy}})(\text{PPh}_2(\text{C}_6\text{H}_4\text{COOH}))][\text{CF}_3\text{SO}_3]$ (4). Yield: 50% (78 mg). Orange single crystals were obtained from slow diffusion of *n*-hexane into tetrahydrofuran solution.

^1H NMR $[(\text{CD}_3)_2\text{SO}, \text{Me}_4\text{Si}]$ δ (ppm): 13.19 (s br, 1H, COOH), 9.28 (d, 2H, $^3J_{\text{HH}} = 6$, H6), 7.98 (s, 2H, H3), 7.76 (d, 2H, $^3J_{\text{HH}} = 8$, Hm'), 7.43 (t,

2H, $^3J_{\text{HH}} = 8$, Hp), 7.33 (t, 4H, $^3J_{\text{HH}} = \text{Ho}$) 7.18 (d, 2H, $^3J_{\text{HH}} = 8$, H5), 7.04 (t, 4H, $^3J_{\text{HH}} = 8$, Hm), 6.93 (t, 2H, $^3J_{\text{HH}} = 8$, Ho'), 5.62 (m, 2H, CH_2OH), 4.84 (s, 5H, C_5H_5), 4.58 (s br, 4H, CH_2OH). APT- $^{13}\text{C}\{^1\text{H}\}$ NMR $[(\text{CD}_3)_2\text{SO}]$ δ (ppm): 166.8 (COOH), 155.5 (br, C6), 154.8 (C2), 152.8 (C4), 133.8 (d, $^1J_{\text{CP}} = 38$, Ci'), 132.8 (d, $^2J_{\text{CP}} = 12$, Co), 132.4 (d, $^2J_{\text{CP}} = 12$, Co'), 131.6 (Cp'), 131.0 (d, $^1J_{\text{CP}} = 42$, Ci), 130.7 (br, Cp), 128.9 (d, $^3J_{\text{CP}} = 10$, Cm'), 128.6 (d, $^3J_{\text{CP}} = 10$, Cm), 122.4 (C5), 120.2 (C3), 78.2 (d, $^2J_{\text{CP}} = 2$, C_5H_5), 60.9 (CH_2OH). $^{31}\text{P}\{^1\text{H}\}$ NMR $[(\text{CD}_3)_2\text{SO}]$ δ (ppm): 52.1 (s, $\text{PPh}_2(\text{C}_6\text{H}_4\text{COOH})$). FTIR [KBr, cm^{-1}]: 3390 ($\nu_{\text{O-H}}$), 3074–2974 ($\nu_{\text{C-H}}$ aromatic rings), 2870 ($\nu_{\text{C-H}}$ alkanes), 1718 ($\nu_{\text{C=O}}$), 1435 ($\nu_{\text{C=C}}$ aromatic rings), 1282 ($\nu_{\text{CF}_3\text{SO}_3}$ counterion). UV–Vis [DMSO, $\lambda_{\text{max}}/\text{nm}$ ($\epsilon \times 10^3/\text{M}^{-1}\text{cm}^{-1}$): 292 (18.99), 371 (sh), 413 (sh), 482 (sh). UV–Vis [CH_2Cl_2 , $\lambda_{\text{max}}/\text{nm}$ ($\epsilon \times 10^3/\text{M}^{-1}\text{cm}^{-1}$): 260 (15.69), 294 (16.64), 362 (sh), 416 (sh), 474 (sh). Elemental analysis calc. for $\text{C}_{37}\text{H}_{32}\text{F}_3\text{N}_2\text{O}_7\text{PRuS}$ (837.76 g mol^{-1}): C, 53.05; H, 3.85; N, 3.34; S, 3.83. Found: C, 53.2; H, 4.0; N, 3.5; S, 4.1. ESI-MS: $[\text{4-CF}_3\text{SO}_3] + \text{calc. for } [\text{C}_{36}\text{H}_{32}\text{N}_2\text{O}_4\text{PRu}] +$: 689.11, found: 689.02 (100 %).

4.3.2.5. $[\text{Ru}(\eta^5\text{-C}_5\text{H}_5)(4,4'\text{-CH}_2\text{-biotin-2,2'-bipy})(\text{PPh}_2(\text{C}_6\text{H}_4\text{COOH}))][\text{CF}_3\text{SO}_3]$ (**5**). Yield: 41% (97 mg).

^1H NMR $[(\text{CD}_3)_2\text{SO}, \text{Me}_4\text{Si}]$ δ (ppm): 13.22 (s br, 1H, COOH), 9.36 (m, 2H, H6), 8.08 (s, 2H, H3), 7.74 (d, 2H, $^3J_{\text{HH}} = 8$, Hm'), 7.43 (t, 2H, $^3J_{\text{HH}} = 8$, Hp), 7.33 (t, 4H, $^3J_{\text{HH}} = 8$, Ho) 7.18 (d, 2H, $^3J_{\text{HH}} = 8$, H5), 7.03 (t, 4H, $^3J_{\text{HH}} = 8$, Hm), 6.87 (t, 2H, $^3J_{\text{HH}} = 8$, Ho'), 5.16 (s, 2H, CH_2Biotin), 4.89 (s, 5H, C_5H_5), 4.31 ($\text{SCH}_2\text{-CH}^{\text{Biotin}}$), 4.14 (m, 4H, $\text{CH}^{\text{Biotin}}$), 3.10 (m, 2H, $\text{S-CH}^{\text{Biotin}}$), 2.81 (m, 2H, $\text{SCH}_2^{\text{Biotin}}$), 2.59 (m, 2H, $\text{SCH}_2^{\text{Biotin}}$), 2.46* + 1.62–1.36 (3 x m, 14H, $\text{CH}_2\text{CH}_2\text{CH}_2\text{CH}_2^{\text{Biotin}}$). * under the solvent residual peak. APT- $^{13}\text{C}\{^1\text{H}\}$ NMR $[(\text{CD}_3)_2\text{SO}]$ δ (ppm): 173.1 (CO , urea biotin), 167.3 (COOH), 163.3 (CO , ester biotin), 156.3 (br, C6), 155.3 (C2), 146.6 (C4), 136.3 (d, $^1J_{\text{CP}} = 38$, Ci'), 133.1 (d, $^2J_{\text{CP}} = 12$, Co), 132.2 (d, $^2J_{\text{CP}} = 12$, Co'), 131.6 (Cp'), 131.2 (d, $^1J_{\text{CP}} = 42$, Ci), 130.3 (br, Cp), 128.9 (d, $^3J_{\text{CP}} = 10$, Cm'), 128.6 (d, $^3J_{\text{CP}} = 10$, Cm), 123.8 (C5), 122.0 (C3), 78.9 (d, $^2J_{\text{CP}} = 2$, C_5H_5), 67.5 ($\text{bipy-CH}_2\text{Biotin}$), 63.5 ($\text{SCHCH}^{\text{Biotin}}$), 61.5 ($\text{CH}^{\text{Biotin}}$), 59.7 ($\text{SCH}_2\text{-CH}^{\text{Biotin}}$), 55.8 ($\text{SCH}^{\text{Biotin}}$), 34.8 ($\text{SCH}_2^{\text{Biotin}}$), 39.9* + 33.5 + 28.5 + 24.9 ($\text{CH}_2\text{CH}_2\text{CH}_2\text{CH}_2^{\text{Biotin}}$). * Under the signal of the solvent. $^{31}\text{P}\{^1\text{H}\}$ NMR $[(\text{CD}_3)_2\text{SO}]$ δ (ppm): 52.3 (s, $\text{PPh}_2(\text{C}_6\text{H}_4\text{COOH})$). FTIR [KBr, cm^{-1}]: 3328 ($\nu_{\text{N-H}}$), 3072–3024 ($\nu_{\text{C-H}}$ aromatic rings), 2931–2862 ($\nu_{\text{C-H}}$ alkanes), 1735–1697 ($\nu_{\text{C=O}}$, acid, ester e urea), 1435 ($\nu_{\text{C=C}}$ aromatic rings), 1276 ($\nu_{\text{CF}_3\text{SO}_3}$ counterion). UV–Vis [DMSO, $\lambda_{\text{max}}/\text{nm}$ ($\epsilon \times 10^3/\text{M}^{-1}\text{cm}^{-1}$): 297 (24.89), 364 (sh), 421 (4.34), 483 (sh). UV–Vis [CH_2Cl_2 , $\lambda_{\text{max}}/\text{nm}$ ($\epsilon \times 10^3/\text{M}^{-1}\text{cm}^{-1}$): 249 (24.63), 292 (23.37), 352 (6.83), 429 (4.26), 493 (sh). Elemental analysis calc. for $\text{C}_{57}\text{H}_{60}\text{F}_3\text{N}_6\text{O}_{11}\text{PRuS}_3$ (1290.22 g mol^{-1}): C, 53.06; H, 4.69; N, 6.51; S, 7.45. Found: C, 52.8; H, 4.8; N, 6.7; S, 7.8. ESI-MS: $[\text{5-CF}_3\text{SO}_3] + \text{calc. for } [\text{C}_{56}\text{H}_{60}\text{N}_6\text{O}_8\text{PRuS}_2] +$: 1141.27, found: 1141.99 (100 %).

4.3.3. Synthesis of the complexes $[\text{Ru}(\eta^5\text{-C}_5\text{H}_5)(\text{bipy-R})(\text{PPh}_2(\text{C}_6\text{H}_4\text{COOCH}_2\text{CH}_2\text{OH}))][\text{CF}_3\text{SO}_3]$ (**6–10**)

Complexes of general formula $[\text{Ru}(\eta^5\text{-C}_5\text{H}_5)(\text{bipy-R})(\text{PPh}_2(\text{C}_6\text{H}_4\text{COOCH}_2\text{CH}_2\text{OH}))][\text{CF}_3\text{SO}_3]$ (**6–10**) were prepared by treating the parent cationic compound $[\text{Ru}(\eta^5\text{-C}_5\text{H}_5)(\text{bipy-R})(\text{PPh}_2(\text{C}_6\text{H}_4\text{COOH}))][\text{CF}_3\text{SO}_3]$ (100 mg, 0.08–0.13 mmol) with EDC•Cl (48–50 mg, 0.25 mmol), DMAP (6–10 mg, 0.05–0.08 mmol) and ethylene glycol (0.25 mL, 4.5 mmol) in THF (5 mL). The orange solutions were stirred at room temperature overnight (up to 20 h), then the solvent was removed under vacuum. The residue obtained was thoroughly washed with water (3 \times 15 mL), *n*-hexane (2 \times 10 mL) and recrystallized from acetone/*n*-hexane (**6** and **7**) or dichloromethane/ether (**8**, **9**, and **10**) to give orange foamy solids.

4.3.3.1. $[\text{Ru}(\eta^5\text{-C}_5\text{H}_5)(2,2'\text{-bipy})(\text{PPh}_2(\text{C}_6\text{H}_4\text{COOCH}_2\text{CH}_2\text{OH}))][\text{CF}_3\text{SO}_3]$ (**6**). Yield: 53 % (56 mg).

^1H NMR $[(\text{CD}_3)_2\text{SO}, \text{Me}_4\text{Si}]$ δ (ppm): 9.37 (d, 2H, $^3J_{\text{HH}} = 4$, H6), 8.19 (d, 2H, $^3J_{\text{HH}} = 8$, H3), 7.86 (m, 4H, $\text{H4} + \text{Hm'}$), 7.41 (t, 2H, $^3J_{\text{HH}} = 8$,

Hp), 7.31 (m, 6H, $\text{Ho} + \text{H5}$), 7.10 (t, 2H, $^3J_{\text{HH}} = 8$, Ho'), 6.94 (m, 4H, Hm), 4.90 (s + t, 6H, C_5H_5 and $-\text{COOCH}_2\text{CH}_2\text{OH}$), 4.29 (t, 2H, $^3J_{\text{HH}} = 5$, $-\text{COOCH}_2\text{CH}_2\text{OH}$), 3.70 (m, 2H, $-\text{COOCH}_2\text{CH}_2\text{OH}$). APT- $^{13}\text{C}\{^1\text{H}\}$ NMR $[(\text{CD}_3)_2\text{SO}]$ δ (ppm): 165.3 ($-\text{COOCH}_2\text{CH}_2\text{OH}$), 156.1 (d, $^2J_{\text{CP}} = 2$, C6), 155.2 (C2), 137.1 (d, $^1J_{\text{CP}} = 38$, Ci'), 136.3 (C4), 132.9 (d, $^2J_{\text{CP}} = 11$, Co'), 132.6 (d, $^2J_{\text{CP}} = 11$, Co), 131.0 (d, $^4J_{\text{CP}} = 2$, Cp'), 130.6 (d, $^1J_{\text{CP}} = 42$, Ci), 130.3 (d, $^4J_{\text{CP}} = 2$, Cp), 129.0 (d, $^3J_{\text{CP}} = 10$, Cm'), 128.6 (d, $^3J_{\text{CP}} = 10$, Cm), 125.2 (C5), 123.5 (C3), 78.6 (d, $^2J_{\text{CP}} = 1$, C_5H_5), 66.8 ($-\text{COOCH}_2\text{CH}_2\text{OH}$), 59.1 ($-\text{COOCH}_2\text{CH}_2\text{OH}$). $^{31}\text{P}\{^1\text{H}\}$ NMR $[(\text{CD}_3)_2\text{SO}]$ δ (ppm): 51.2 (s, $\text{PPh}_2(\text{C}_6\text{H}_4\text{COOCH}_2\text{CH}_2\text{OH})$). FTIR [KBr, cm^{-1}]: 3452 ($\nu_{\text{O-H}}$), 3107–3077 ($\nu_{\text{C-H}}$ aromatic rings), 2951–2880 ($\nu_{\text{C-H}}$ alkanes), 1718 ($\nu_{\text{C=O}}$), 1436 ($\nu_{\text{C=C}}$ aromatic rings), 1268 ($\nu_{\text{CF}_3\text{SO}_3}$ counterion). UV–Vis [DMSO, $\lambda_{\text{max}}/\text{nm}$ ($\epsilon \times 10^3/\text{M}^{-1}\text{cm}^{-1}$): 290 (19.61), 371 (sh), 422 (sh), 478 (sh). UV–Vis [CH_2Cl_2 , $\lambda_{\text{max}}/\text{nm}$ ($\epsilon \times 10^3/\text{M}^{-1}\text{cm}^{-1}$): 289 (24.23), 355 (sh), 417 (4.44), 420 (sh). Elemental analysis calc. for $\text{C}_{37}\text{H}_{32}\text{F}_3\text{N}_2\text{O}_6\text{PRuS}$ (821.76 g mol^{-1}): 54.08; H, 3.92; N, 3.41; S, 3.90. Found: C, 53.9; H, 3.9; N, 3.5; S, 4.0. ESI-MS: $[\text{6-CF}_3\text{SO}_3] + \text{calc. for } [\text{C}_{36}\text{H}_{32}\text{N}_2\text{O}_3\text{PRu}] +$: 673.12, found: 673.05 (100 %).

4.3.3.2. $[\text{Ru}(\eta^5\text{-C}_5\text{H}_5)(4,4'\text{-CH}_3\text{-bipy})(\text{PPh}_2(\text{C}_6\text{H}_4\text{COOCH}_2\text{CH}_2\text{OH}))][\text{CF}_3\text{SO}_3]$ (**7**). Yield: 50% (54 mg).

^1H NMR $[(\text{CD}_3)_2\text{SO}, \text{Me}_4\text{Si}]$ δ (ppm): 9.17 (d, 2H, $^3J_{\text{HH}} = 6$, H6), 8.01 (s, 2H, H3), 7.83 (d, 2H, $^3J_{\text{HH}} = 8$, Hm'), 7.43 (t, 2H, $^3J_{\text{HH}} = 8$, Hp), 7.33 (t, 4H, $^3J_{\text{HH}} = 8$, Ho), 7.18 (d, 2H, $^3J_{\text{HH}} = 8$, H5), 7.02 (m, 6H, $\text{Hm} + \text{Ho'}$), 4.93 (t, 1H, $^3J_{\text{HH}} = 5$, $-\text{COOCH}_2\text{CH}_2\text{OH}$), 4.83 (s, 5H, C_5H_5), 4.30 (t, 2H, $^3J_{\text{HH}} = 5$, $-\text{COOCH}_2\text{CH}_2\text{OH}$), 3.70 (m, 2H, $-\text{COOCH}_2\text{CH}_2\text{OH}$), 2.38 (s, 6H, CH_3). APT- $^{13}\text{C}\{^1\text{H}\}$ NMR $[(\text{CD}_3)_2\text{SO}]$ δ (ppm): 165.3 ($-\text{COOCH}_2\text{CH}_2\text{OH}$), 155.3 (br, C6), 154.9 (C2), 148.1 (C4), 137.1 (d, $^1J_{\text{CP}} = 38$, Ci'), 132.8 (d, $^2J_{\text{CP}} = 12$, Co), 132.4 (d, $^2J_{\text{CP}} = 12$, Co'), 131.6 (Cp'), 131.2 (d, $^1J_{\text{CP}} = 42$, Ci), 130.3 (br, Cp), 128.9 (d, $^3J_{\text{CP}} = 10$, Cm'), 128.6 (d, $^3J_{\text{CP}} = 10$, Cm), 126.1 (C5), 123.9 (C3), 78.1 (d, $^2J_{\text{CP}} = 1$, C_5H_5), 66.8 ($-\text{COOCH}_2\text{CH}_2\text{OH}$), 59.1 ($-\text{COOCH}_2\text{CH}_2\text{OH}$), 20.3 (CH_3). $^{31}\text{P}\{^1\text{H}\}$ NMR $[(\text{CD}_3)_2\text{SO}]$ δ (ppm): 52.3 (s, $\text{PPh}_2(\text{C}_6\text{H}_4\text{COOCH}_2\text{CH}_2\text{OH})$). FTIR [KBr, cm^{-1}]: 3452 ($\nu_{\text{O-H}}$), 3059 ($\nu_{\text{C-H}}$ aromatic rings), 2953–2874 ($\nu_{\text{C-H}}$ alkanes), 1720 ($\nu_{\text{C=O}}$), 1435 ($\nu_{\text{C=C}}$ aromatic rings), 1276 ($\nu_{\text{CF}_3\text{SO}_3}$ counterion). UV–Vis [DMSO, $\lambda_{\text{max}}/\text{nm}$ ($\epsilon \times 10^3/\text{M}^{-1}\text{cm}^{-1}$): 293 (18.91), 374 (sh), 420 (sh), 476 (sh). UV–Vis [CH_2Cl_2 , $\lambda_{\text{max}}/\text{nm}$ ($\epsilon \times 10^3/\text{M}^{-1}\text{cm}^{-1}$): 285 (24.72), 362 (sh), 417 (5.11), 471 (sh). Elemental analysis calc. for $\text{C}_{39}\text{H}_{36}\text{F}_3\text{N}_2\text{O}_6\text{PRuS}$ (849.82 g mol^{-1}): C, 55.12; H, 4.27; N, 3.30; S, 3.77. Found: C, 55.0; H, 4.3; N, 3.5; S, 3.7. ESI-MS: $[\text{7-CF}_3\text{SO}_3] + \text{calc. for } [\text{C}_{38}\text{H}_{36}\text{N}_2\text{O}_3\text{PRu}] +$: 701.15, found: 701.04 (100 %).

4.3.3.3. $[\text{Ru}(\eta^5\text{-C}_5\text{H}_5)(4,4'\text{-OCH}_3\text{-2,2'-bipy})(\text{PPh}_2(\text{C}_6\text{H}_4\text{COOCH}_2\text{CH}_2\text{OH}))][\text{CF}_3\text{SO}_3]$ (**8**). Yield: 57% (61 mg).

^1H NMR $[(\text{CD}_3)_2\text{SO}, \text{Me}_4\text{Si}]$ δ (ppm): 9.06 (d, 2H, $^3J_{\text{HH}} = 6$, H6), 8.01 (s, 2H, H3), 7.83 (d, 2H, $^3J_{\text{HH}} = 8$, Hm'), 7.43 (t, 2H, $^3J_{\text{HH}} = 8$, Hp), 7.33 (t, 4H, $^3J_{\text{HH}} = 8$, Ho), 7.19 (d, 2H, $^3J_{\text{HH}} = 8$, H5), 7.02 (t, 4H, $^3J_{\text{HH}} = 8$, Hm), 6.85 (t, 2H, $^3J_{\text{HH}} = 8$, Ho'), 4.93 (t, 1H, $^3J_{\text{HH}} = 5$, $-\text{COOCH}_2\text{CH}_2\text{OH}$), 4.78 (s, 5H, C_5H_5), 4.29 (t, 2H, $^3J_{\text{HH}} = 5$, $-\text{COOCH}_2\text{CH}_2\text{OH}$), 3.90 (m, 2H, $-\text{COOCH}_2\text{CH}_2\text{OH}$), 3.89 (s, 6H, $-\text{OCH}_3$). APT- $^{13}\text{C}\{^1\text{H}\}$ NMR $[(\text{CD}_3)_2\text{SO}]$ δ (ppm): 165.9 ($-\text{COOCH}_2\text{CH}_2\text{OH}$), 165.4 (C6), 156.7 (C2), 156.6 (C4), 137.8 (d, $^1J_{\text{CP}} = 38$, Ci'), 133.8 (d, $^2J_{\text{CP}} = 12$, Co'), 132.8 (d, $^2J_{\text{CP}} = 12$, Co), 131.4 (d, $^1J_{\text{CP}} = 42$, Ci), 130.8 (Cp'), 130.2 (br, Cp), 129.1 (d, $^3J_{\text{CP}} = 10$, Cm'), 128.6 (d, $^3J_{\text{CP}} = 10$, Cm), 112.4 (C5), 109.8 (C3), 77.5 (d, $^2J_{\text{CP}} = 2$, C_5H_5), 66.8 ($-\text{COOCH}_2\text{CH}_2\text{OH}$), 59.1 ($-\text{COOCH}_2\text{CH}_2\text{OH}$), 56.6 ($-\text{OCH}_3$). $^{31}\text{P}\{^1\text{H}\}$ NMR $[(\text{CD}_3)_2\text{SO}]$ δ (ppm): 52.9 (s, $\text{PPh}_2(\text{C}_6\text{H}_4\text{COOCH}_2\text{CH}_2\text{OH})$). FTIR [KBr, cm^{-1}]: 3441 ($\nu_{\text{O-H}}$), 3076 ($\nu_{\text{C-H}}$ aromatic rings), 2947–2880 ($\nu_{\text{C-H}}$ alkanes), 1718 ($\nu_{\text{C=O}}$), 1435 ($\nu_{\text{C=C}}$ aromatic rings), 1268 ($\nu_{\text{CF}_3\text{SO}_3}$ counterion). UV–Vis [DMSO, $\lambda_{\text{max}}/\text{nm}$ ($\epsilon \times 10^3/\text{M}^{-1}\text{cm}^{-1}$): 290 (17.99), 370 (sh), 410 (sh), 470 (sh). UV–Vis [CH_2Cl_2 , $\lambda_{\text{max}}/\text{nm}$ ($\epsilon \times 10^3/\text{M}^{-1}\text{cm}^{-1}$): 261 (18.31), 289 (19.98), 362 (sh), 415 (sh), 470 (sh). Elemental analysis calc. for $\text{C}_{39}\text{H}_{36}\text{F}_3\text{N}_2\text{O}_8\text{PRuS}$ (881.82 g mol^{-1}): C, 53.12; H, 4.11; N, 3.18; S, 3.64. Found: C, 53.1; H, 4.1; N, 3.0; S, 3.5. ESI-MS: $[\text{8-CF}_3\text{SO}_3] + \text{calc. for } [\text{C}_{38}\text{H}_{36}\text{N}_2\text{O}_5\text{PRu}] +$: 733.14, found: 732.98 (100 %).

4.3.3.4. [Ru(η^5 -C₅H₅)(4,4'-CH₂OH-2,2'-bipy)

(PPh₂(C₆H₄COOCH₂CH₂OH))][CF₃SO₃] (**9**). Yield: 45% (47 mg).

¹H NMR [(CD₃)₂SO, Me₄Si] δ (ppm): 9.28 (d, 2H, ³J_{HH} = 6, H₆), 7.98 (s, 2H, H₃), 7.85 (d, 2H, ³J_{HH} = 8, H_m'), 7.50 (t, 2H, ³J_{HH} = 8, H_p), 7.35 (t, 4H, ³J_{HH} = 8, H_o), 7.34 (d, 2H, ³J_{HH} = 8, H₅), 7.07 (t, 2H, ³J_{HH} = 8, H_o'), 6.98 (t, 4H, ³J_{HH} = 8, H_m), 5.63 (m, 2H, CH₂OH), 4.93 (t, 1H, ³J_{HH} = 5, -COOCH₂CH₂OH), 4.85 (s, 5H, C₅H₅), 4.60 (s, 4H, CH₂OH), 4.28 (t, 2H, ³J_{HH} = 4, -COOCH₂CH₂OH), 3.68 (m, 2H, -COOCH₂CH₂OH). APT-¹³C{¹H} NMR [(CD₃)₂SO] δ (ppm): 165.3 (-COOCH₂CH₂OH), 155.5 (C₆), 154.8 (C₂), 152.8 (C₄), 137.4 (d, ¹J_{CP} = 38, C_i'), 133.8 (d, ²J_{CP} = 12, C_o'), 132.8 (d, ²J_{CP} = 12, C_o), 131.0 (C_p'), 130.9 (d, ¹J_{CP} = 42, C_i), 130.2 (br, C_p), 129.2 (d, ³J_{CP} = 10, C_m'), 128.6 (d, ³J_{CP} = 10, C_m), 122.5 (C₅), 120.2 (C₃), 78.2 (d, ²J_{CP} = 2, C₅H₅), 66.8 (-COOCH₂CH₂OH), 61.0 (-CH₂OH), 59.1 (-COOCH₂CH₂OH). ³¹P{¹H} NMR [(CD₃)₂SO] δ (ppm): 52.2 (s, PPh₂(C₆H₄COOCH₂CH₂OH)). FTIR [KBr, cm⁻¹]: 3418 (ν_{O-H}), 3073–3040 (ν_{C-H} aromatic rings), 2926–2870 (ν_{C-H} alkanes), 1718 ($\nu_{C=O}$), 1435 ($\nu_{C=C}$ aromatic rings), 1270 ($\nu_{CF_3SO_3}$ counterion). UV–Vis [DMSO, λ_{max}/nm ($\epsilon \times 10^3/M^{-1}cm^{-1}$): 292 (18.99), 371 (sh), 413 (sh), 482 (sh). UV–Vis [CH₂Cl₂, λ_{max}/nm ($\epsilon \times 10^3/M^{-1}cm^{-1}$): 260 (15.69), 294 (16.64), 362 (sh), 416 (sh), 474 (sh). Elemental analysis calc. for C₃₉H₃₆F₃N₂O₈PRuS (881.82 g/mol): C, 53.12; H, 4.11; N, 3.18; S, 3.64. Found: C, 53.2; H, 4.2; N, 3.5; S, 4.0. ESI-MS: [9-CF₃SO₃]+ calc. for [C₃₈H₃₆N₂O₅PRu]+: 733.14, found: 733.02 (100 %).

4.3.3.5. [Ru(η^5 -C₅H₅)(4,4'-CH₂-biotin-2,2'-bipy)

(PPh₂(C₆H₄COOCH₂CH₂OH))][CF₃SO₃] (**10**). Yield: 38% (40 mg).

¹H NMR [(CD₃)₂SO, Me₄Si] δ (ppm): 9.36 (m, 2H, H₆), 8.08 (s, 2H, H₃), 7.88 (d, 2H, ³J_{HH} = 8, H_m'), 7.42 (t, 2H, ³J_{HH} = 8, H_p), 7.31 (t, 4H, ³J_{HH} = 8, H_o), 7.10 (t, 2H, ³J_{HH} = 8, H_o'), 6.96 (t, 4H, ³J_{HH} = 8, H_m), 6.48–6.42 (NH-Biotin), 5.17 (s, 4H, CH₂Biotin), 4.93–4.91 (s + t, 6H, C₅H₅ + -COOCH₂CH₂OH), 4.30 (m, 4H, -COOCH₂CH₂OH + CH₂Biotin), 4.31 (m, 2H, SCH₂-CH₂Biotin), 3.71 (m, 2H, -COOCH₂CH₂OH), 3.10 (m, 2H, S-CH₂Biotin), 2.81 (m, 2H, SCH₂Biotin), 2.59 (m, 2H, SCH₂Biotin), 2.46* + 1.62–1.36 (3 x m, 14H, CH₂CH₂CH₂CH₂Biotin). * Under the solvent residual peak. APT-¹³C{¹H} NMR [(CD₃)₂SO] δ (ppm): 173.1 (CO, urea biotin), 165.7 (COOCH₂CH₂OH), 163.3 (CO, ester biotin), 156.3 (br, C₆), 155.3 (C₂), 146.7 (C₄), 137.1 (d, ¹J_{CP} = 38, C_i'), 134.2 (d, ²J_{CP} = 12, C_o), 132.2 (d, ²J_{CP} = 12, C_o'), 131.6 (C_p'), 131.2 (d, ¹J_{CP} = 42, C_i), 130.3 (br, C_p), 128.9 (d, ³J_{CP} = 10, C_m'), 129.3 (d, ³J_{CP} = 10, C_m), 123.7 (C₅), 122.0 (C₃), 79.0 (d, ²J_{CP} = 2, C₅H₅), 67.3 (bipy-CH₂Biotin), 63.6 (br, SCH₂-CH₂Biotin + COOCH₂CH₂OH), 61.5 (CH₂Biotin), 59.7 (SCH₂-CH₂Biotin + COOCH₂CH₂OH), 55.9 (SCH₂Biotin), 34.8 (SCH₂Biotin), 39.9 + 33.5 + 28.5 + 24.9 (CH₂CH₂CH₂CH₂Biotin). * Under the signal of the solvent. ³¹P{¹H} NMR [(CD₃)₂SO] δ (ppm): 52.1 (s, PPh₂(C₆H₄COOCH₂CH₂OH)). FTIR [KBr, cm⁻¹]: 3450–3390 (ν_{O-H} and ν_{N-H}), 3100–3040 (ν_{C-H} aromatic rings), 2929–2895 (ν_{C-H} aliphatics), 1720–1699 (shoulder, $\nu_{C=O}$), 1264 ($\nu_{CF_3SO_3}$ counterion), 1186 (ν_{C-O} ester), 1030 (ν_{N-C} amine). UV–Vis [DMSO, λ_{max}/nm ($\epsilon \times 10^3/M^{-1}cm^{-1}$): 293 (19.46), 370 (sh), 421 (sh), 481 (sh). UV–Vis [CH₂Cl₂, λ_{max}/nm ($\epsilon \times 10^3/M^{-1}cm^{-1}$): 250 (22.31), 288 (20.87), 368 (sh), 417 (sh), 480 (sh). Elemental analysis calc. for C₅₉H₆₄F₃N₆O₁₂PRuS₃ (1334.41 g/mol): C, 53.10; H, 4.83; N, 6.30; S, 7.21. Found: C, 52.9; H, 5.0; N, 6.2; S, 7.0. ESI-MS: [10-CF₃SO₃]+ calc. for [C₅₈H₆₄N₆O₉PRuS₂]+: 1185.34, found: 1185.00 (100 %).

4.4. X-ray structure analysis

The X-ray intensity data were measured on a D8 QUEST ECO three-circle diffractometer system equipped with a Ceramic X-ray tube (Mo K α , λ = 0.71076 Å) and a doubly curved silicon crystal monochromator, using APEX3 [40] software package. The frames were integrated with the Bruker SAINT [41]. Data were corrected for absorption effects using the Multi-Scan method (SADABS) [42]. The structures were solved and refined using the Bruker SHELXTL [43].

The crystallographic data as well as details of the structure solution

and refinement procedures are reported in supplementary information. CCDC 2278188 (for [Ru(η^5 -C₅H₅)(PPh₂(C₆H₄COOH))₂Cl]), 2278189 (for (**1**)), 2278191 (for (**3**)) and 2278190 (for (**4**)) contain the supplementary crystallographic data for this paper. These data can be obtained free of charge from The Cambridge Crystallographic Data Centre via www.ccdc.cam.ac.uk/products/csd/request/

4.5. UV–vis spectroscopy

A Thermo Evolution 220 spectrophotometer was used to record the UV–Vis spectra in the 260–700 nm wavelength region, the path length was 1, 2 or 5 cm. For the stability studies, all complexes were dissolved in 100% DMSO (or 100% DMSO-*d*₆) and a sample containing each compound in 2% DMSO/Eagle's minimum essential medium (EMEM) (buffered at pH 7.4) up to 200 μ M was prepared. Their electronic spectra were recorded in the range allowed by the solvent mixture at set time intervals. Samples were stored at room temperature and protected from light between measurements. The variation percentage between UV–Vis measurements were calculated by the following expression:

$$\% \text{ variation} = \frac{Abs(\lambda, t_{mix}) - Abs(\lambda, t_{mix} + i)}{Abs(t_{mix})} \times 100$$

Spectrophotometric titrations were applied to study the proton dissociation in 30% (v/v) DMSO/water mixture due to the limited aqueous solubility of the compounds. The calibration of the electrode system was performed by strong acid – strong base pH-potentiometric titrations in 30% (v/v) DMSO/H₂O solvent mixture at 25.0 \pm 0.1 °C as described in our previous works [44]. 0.1 M KCl was the supporting electrolyte to maintain constant ionic strength, which refers to the chloride ion concentration in blood plasma. Proton dissociation constant (*K*_a) of the complexes were determined using low concentration (12–30 μ M) of the compounds. The starting sample volume was 10 mL. Spectrophotometric titrations were performed in the pH range 1.8–9.0 for 30% (v/v) DMSO/H₂O medium. Prior to the titrations purified argon was passed through the samples for approximately 10 min to remove carbon-dioxide traces and argon was also passed over the samples during these measurements. The proton dissociation constants were calculated by using the computer program PSEQUAD [27]. The reactions between the title compounds with DNA were also followed by UV–Vis spectroscopy. Samples contained the metal complexes in low concentration (~20 μ M) and 2% (v/v) DMSO/phosphate buffer solution (pH = 7.4) was applied to avoid precipitation.

4.6. ¹H and ³¹P{¹H}-NMR spectroscopy

¹H and ³¹P NMR studies were carried out on a Bruker Ultrashield 500 Plus instrument (Billerica, MA, USA) to follow the stability of the complexes in solution. DSS and H₃PO₄ were used as an internal NMR standards and WATERGATE water suppression pulse scheme was used. Spectra were recorded in DMSO-*d*₆ and in 30% (v/v) DMSO-*d*₆/H₂O solvent mixtures at ionic strength of 0.1 M KCl.

4.7. Spectrofluorometry

Fluorescence studies were measured using a Fluoromax fluorometer (Horiba Jobin Yvon) in 1 cm quartz cells. The interaction of the complexes with DNA was measured through ethidium bromide (EB) displacement, while interaction with human serum albumin (HSA) was followed by the competition of the site marker dansylglycine (DG) with the metal complexes. In these setups, the DNA(base pairs):EB:metal complex ratio was varied between 2:1:0 and 2:1:10, and similarly, the HSA:DG:metal complex ratio was varied between 1:1:0 to 1:1:5, where the concentration of the complexes was varied up to 5 \times excess compared to the macromolecule concentration. Instrumental settings are collected in Table S4. Spectra were corrected with self-absorbance and the inner filter effect, as it is suggested by Lakowicz [45].

The same fluorometer is also equipped with a DeltaHub time-correlated single photon counting (TCSPC) controller, having a NanoLED light source N-360 (Horiba Jobin Yvon). The fluorescence lifetime measurements were measured with the instrument settings in Table S5. A Ludox® scatter solution (Sigma-Aldrich) was used to obtain the instrument response function. The signal of blank sample was subtracted from the decay. For analysis the software DAS6 (version 6.6.; Horiba Jobin Yvon) was used to evaluate the experimental fluorescence decays. The intensity decay is described by a sum of exponentials as the function of time (Equation (1)):

$$I(t) = \sum_{i=1}^n \alpha_i \exp\left(\frac{-t}{\tau_i}\right) \quad \text{Equation 1}$$

where α_i is the normalized amplitude of the i component and τ_i is its lifetime. The experimental data for fluorescence intensity decay curve was described as the sum of two exponentials ($n = 2$ in Equation (1)) with fitted lifetime components (τ_1 and τ_2) and with normalized amplitudes (α_1 and α_2 ($\alpha_1 = 1 - \alpha_2$)). Using these parameters, the fraction of light (f_i) and the amplitude-weighted average lifetime (τ_{av}) can be calculated by Equations 2 and 3, respectively:

$$f_i = \frac{\alpha_i \tau_i}{\sum_{i=1}^n (\alpha_i \tau_i)} \quad \text{Equation 2}$$

$$\tau_{av} = \sum_{i=1}^n \alpha_i \tau_i \quad \text{Equation 3}$$

The quality of the fit was acceptable, when χ^2_R was less than 1.20, and the weighted residuals had a random distribution. Decay curves were recorded at 360 nm. Global fitting was applied for evaluation; τ of the DG was kept constant (τ_1 fitted from a separate measurement under the same conditions); α_1 , α_2 and τ_2 values were refined.

4.8. Lipophilicity and thermodynamic solubility measurements

The distribution coefficient values ($D_{7.4}$) were determined by the traditional shake-flask method in n -octanol/buffered aqueous solution at pH 7.40 (20 mM phosphate buffer with 0.1 M KCl) at 25.0 ± 0.2 °C. n -Octanol had been pre-saturated with the aqueous buffer solution prior to its use. The stock solutions of the complexes were prepared in n -octanol because of the lower aqueous solubility of some compounds. The aqueous phase: n -octanol phase ratio was different for the different compounds; in the case of the compounds 6–9 it was 3:1, while for compounds 1–4 it was 15:1; for biotin conjugates (5 and 10) a 30:1 ratio was needed due to the high lipophilicity of the latter compounds. Firstly, the phases were mixed with vertical rotation (~ 20 rpm) for 4 h and then they were separated by centrifugation at 6000 rpm for 5 min. After separation, UV–Vis absorption spectra were recorded for both phases. Spectra of the n -octanol phases were compared to the original n -octanol stock solutions, $D_{7.4}$ values were calculated using the spectral range of 250–450 nm. In the case of the complexes with carboxylic acid, the absorption spectrum of compound in the n -octanol phase changed during the shaking due to the deprotonation of the carboxylic function. In these cases, known portions of succinic acid (dissolved in n -octanol) were added to partially protonate the complexes, and $D_{7.4}$ values were calculated at the isosbestic points.

Thermodynamic solubility ($S_{7.4}$) was measured for the saturated solutions in water at pH 7.40 (10 mM phosphate buffer containing 0.1 M KCl) at 25.0 ± 0.2 °C, after one-day shaking. The concentration of the compounds was determined by UV–Vis spectrophotometry using stock solutions of the compounds with known concentration dissolved in 100% DMSO and 50% (v/v) DMSO/buffered aqueous solutions for the calibration.

4.9. Cell lines, culture conditions and in vitro cytotoxicity tests

Cell lines and culture conditions: The cell culture reagents were obtained from Merck and plastic ware from Sarstedt. Human colon Colo 205 (chemo-sensitive, American Type Culture Collection (ATCC) CCL-222), Colo 320 (doxorubicin-resistant, ATCC-CCL-220.1) and human lung A549 (ATCC CCL-185) adenocarcinoma cell lines were purchased from LGC Promochem. The non-small cell lung cancer (NSCLC) cell line NCI-H460, and the non-tumorigenic cell line MCF10A were purchased from ATCC. The NCI-H460/R is a multidrug resistant (MDR) counterpart cell line from NCI-H460, which overexpresses P-gp (a kind gift from Dr. M. Pešić, Belgrade, Serbia) [46,47]. All cancer cells were cultured in RPMI-1640 medium supplemented with 10 % heat-inactivated fetal bovine serum (FBS), 2 mM L-glutamine, 1 mM sodium pyruvate and buffered with 100 mM HEPES. The non-tumorigenic MCF-10A cell line was cultured in DMEM/F12 (Thermo Fischer Scientific, Waltham, MA, USA; 11320033), supplemented with 5 % inactivated Horse Serum (HS; Biowest, Nuaille, France; S0910), 0.5 mg/mL of hydrocortisone (Merck Life Science, Darmstadt, Germany; H0888), 20 ng/mL of human epidermal growth factor (R&D systems, Minneapolis, MN, USA; 236 EG), 10 mg/mL of insulin (Merck Life Science, Darmstadt, Germany; I9278), 100 ng/mL of cholera toxin (Merck Life Science, Darmstadt, Germany; C8052), 100 units/mL penicillin and 100 mg/mL of streptomycin solution (100, Corning Inc., Corning, NY, USA; 30-002-CI), as previously described [48]. The cells were incubated at 37 °C, in a 5 % CO₂, 95 % air atmosphere, and were detached with Trypsin-Versene (EDTA) solution for 5 min at 37 °C.

MTT assay: The tested complexes were dissolved in DMSO using 5 mM concentration. The stock solutions were diluted in complete culture medium. A two-fold serial dilutions of compounds were made in 100 μ L of the medium, horizontally. The semi-adherent colon adenocarcinoma cells were treated with Trypsin-Versene (EDTA) solution. They were adjusted to a density of 1×10^4 cells in 100 μ L of RPMI-1640 medium and were added to each well, with the exception of the medium control wells. In case of the A549 cells, the cells were seeded overnight in 96-well flat-bottomed microtiter plates prior to the assay (1×10^4 cells/well) in EMEM. On the following day the serial dilutions of the compounds were made in a separate plate starting with 100 μ M, and then transferred to the plates containing the A549 cells. The final volume of the wells containing compounds and cells was 200 μ L. The plates containing the cells were incubated at 37 °C for 72 h; at the end of the incubation period, 20 μ L of MTT solution (5 mg/mL) were added to each well. After incubation at 37 °C for 4 h, 100 μ L of sodium dodecyl sulphate solution (10 % in 0.01 M HCl) were added to each well, and the plates were further incubated at 37 °C overnight. Cell growth was determined by measuring the optical density (OD) at 540/630 nm with a Multiskan EX plate reader (Thermo Labsystems). Inhibition of the cell growth (expressed as IC₅₀: inhibitory concentration that reduces by 50 % the growth of the cells exposed to the tested compounds) was determined from the sigmoid curve, where

$$\text{Inhibition} = 100 - ((\text{OD}_{\text{sample}} - \text{OD}_{\text{medium control}})/(\text{OD}_{\text{cell control}} - \text{OD}_{\text{medium control}})) \times 100$$

Values were plotted against the logarithm of compound concentrations. Curves for the data obtained on cancer cells were fitted by GraphPad Prism software [49] using the sigmoidal dose–response model (comparing variable and fixed slopes). The IC₅₀ values were always obtained from at least three independent experiments.

Sulforhodamine B (SRB) Assay: Cells were plated in 96-well plates at a previously determined optimal cell concentration for 24 h (NCI-H460, NCI-H460/R and MCF10-A: 5×10^4 cells/mL); [50,51] and in medium supplemented with 5 % FBS. Then, cells were treated with different concentrations of compounds for 48 h. The SRB assay was performed according to the described protocol [52]. The studies were conducted in two distinct plates: one to be analysed at the time of treatment (T0) and

another to be analysed 48 h later (T48). After a 48 h incubation period, cells were fixed with 10% (w/v) ice-cold trichloroacetic acid (TCA; Merck Life Science, Darmstadt, Germany; T0699) for at least 1 h at 4 °C. After washing with distilled water, cells were allowed to air-dry at room temperature (RT), stained with 0.4% (w/v) SRB (Merck Life Science, Darmstadt, Germany; S9012) in 1% (v/v) acetic acid (Merck Life Science, Darmstadt, Germany; T0699) for 30 min, washed with 1% (v/v) acetic acid to remove the unbound dye and then allowed to air-dry at RT. The bound SRB was solubilized with 10 mM Tris base solution in water (Merck Life Science, Darmstadt, Germany; T6066) and absorbance was measured at 510 nm in a multi plate reader (Synergy™ Mx, Biotek Instruments Inc., Winooski, VT, USA), recurring to the Gen5™ software. In the end, the GI₅₀ concentration (corresponding to 50% of cell growth inhibition) and the cytotoxic effect of the compounds were determined, obtained from at least three independent experiments, using the following formula [53]:

$$\% \text{ growth inhibition} = 100 - ((\text{mean OD}_{\text{sample}} - \text{OD}_{\text{day0}}) / (\text{mean OD}_{\text{negative control}} - \text{mean OD}_{\text{day0}})) \times 100$$

Cell Death Assay: NCI-H460 cells were plated in 6-well plates, at a previously determined optimal cell concentration (5×10^4 cells/mL) [50] and incubated for 24 h. Then, cells were treated with the different compounds for 48 h. Cell death was assessed using the Annexin V-FITC Apoptosis Detection Kit (eBio-science™, Thermo Fisher Scientific, Waltham, MA, USA; BMS500FI), according to manufacturer's instructions and as previously described [50,54]. Briefly, 1 h before cell collection, 100% ethanol was added to the well corresponding to the positive control for necrosis. After collection, cells were centrifuged for 5 min at 1200 rpm at 4 °C and resuspended in the binding buffer solution in water (1X). Cell suspensions were then incubated with the Annexin V-FITC conjugate for 10 min at RT, protected from light. Subsequently, PI was added and samples were analysed using the BD Accuri™ C6 Flow Cytometer and the BDSamples software; after the proper exclusion of cell debris and aggregates, at least 10,000 to 20,000 events per sample were plotted. The flow cytometry results were further analysed using the FlowJo 7.6.5 Software (Tree Star Inc., San Carlos, CA, USA).

Cell cycle profile analysis: NCI-H460 cells were plated in 6-well plates at a previously determined optimal cell concentration (5×10^4 cells/mL) [50] and incubated for 24 h. Then, cells were treated with the different compounds for 48 h. Cell cycle profile was assessed using flow cytometry following propidium iodide (PI) staining, according to manufacturer's instructions and as previously described [34,50,54]. Briefly, cells of each condition were collected, centrifuged (1200 rpm for 5 min at 4 °C) and fixed with ice-cold 70% ethanol (Fischer Scientific, Hampton, NH, USA; E/0650DF/C17) at 4 °C for a period of at least 12 h. Cells were then centrifuged and resuspended in a PBS solution containing 0.1 mg/mL RNase A (Invitrogen, Waltham, MA, USA; 12091021) and 5 µg/mL PI (Merck Life Science, Darmstadt, Germany; 537060) and kept in the dark for at least 30 min. Sample analysis was performed using the BD Accuri™ C6 Flow Cytometer (BD Biosciences, San Jose, CA, USA) and the BDSamples software (BD Biosciences, San Jose, CA, USA), and after the proper exclusion of cell debris and aggregates, at least 10,000 to 20,000 events per sample were plotted. Results were further analysed using the FlowJo 7.6.5 Software (Tree Star Inc., San Carlos, CA, USA).

4.10. Bacterial cell culture and determination of antibacterial effect

Antibacterial activity was determined for all metal complexes in various Gram negative and Gram positive bacterial strains, namely *Klebsiella pneumoniae* (ATCC 700603), *Escherichia coli* (ATCC 25922), *Staphylococcus aureus* (ATCC 25923) and methicillin-resistant *Staphylococcus aureus* (ATCC 43300). The stock solutions of the tested compounds were prepared in DMSO at 5 mM concentration. In parallel, MRSA strains were also treated with reference antibiotics, such as tetracycline, gentamicin and ciprofloxacin, to compare the efficacy of

the title metal complexes to these well-known drugs. All stock solutions were diluted in 100 µL of Mueller Hinton Broth, and then two-fold serial dilutions were performed. Then, 10^{-4} dilution of an overnight bacterial culture in 100 µL of medium was added to each well, with the exception of the medium control wells. The highest concentration of the compounds in the tested samples was 100 µM. The plates were incubated at 37 °C for 18 h. After that, the MIC values were determined by visual inspection. The solvent DMSO did not exert any antibacterial activity. The MIC determination was performed in 4 parallels for each compound and strain, respectively.

Declaration of competing interest

The authors declare that they have no known competing financial interests or personal relationships that could have appeared to influence the work reported in this paper.

Data availability

Data will be made available on request.

Acknowledgements

This work was funded by Fundação para a Ciência e a Tecnologia (FCT), I.P./MCTES through national funds (PIDDAC) - UIDB/00100/2020, UIDP/00100/2020 and LA/P/0056/2020, PTDC/QUI-QIN/28662/2017 and was also supported by the Portuguese-Hungarian Scientific & Technological Cooperation Programme through project TÉT-PT-2018-00002 - FCT/NKFIH 2019/2020. This work was supported by the National Research, Development and Innovation Office-NKFI (Hungary) through project TKP-2021-EGA-32. R. G. Teixeira thanks FCT for his Ph.D. Grant (SFRH/BD/135830/2018 and COVID/BD/153190/2023). A. Valente acknowledges the CEECIND 2017 Initiative (CEE-CIND/01974/2017). G.S. was supported by the János Bolyai Research Scholarship (BO/00158/22/5) of the Hungarian Academy of Sciences and by the ÚNKP-22-5-SZTE-588 New National Excellence Program of the Ministry for Culture and Innovation from the source of the National Research, Development and Innovation Fund.

The Flow Cytometry technique was performed at the Translational Cytometry i3S Scientific Platform with the assistance of Emília Cardoso and Catarina Meireles.

Appendix A. Supplementary data

Supplementary data to this article can be found online at <https://doi.org/10.1016/j.ejmech.2023.115922>.

References

- [1] A.C. Munteanu, V. Uivarosi, *Pharmaceutics* 13 (2021) 1–51.
- [2] A Phase 1b/2a Dose Escalation Study of BOLD-100 in Combination with FOLFOX Chemotherapy in Patients with Advanced Solid Tumours. <https://clinicaltrials.gov/ct2/show/NCT04421820?term=bold100&draw=2&rank=1>, 2023 accessed 29 September 2023.
- [3] A Phase Ib Trial of Intravesical Photodynamic Therapy in Patients with Non-muscle Invasive Bladder Cancer at High Risk of Progression Who Are Refractory to Bacillus Calmette-Guerin Therapy and Who Are Medically Unfit for/Refuse Cystectomy. <https://clinicaltrials.gov/ct2/show/NCT03053635?term=tld1433&draw=2&rank=1>, 2023 accessed 29 September 2023.
- [4] E. Alessio, L. Messori, *Molecules* 24 (2019) 1–20.
- [5] S. Monro, K.L. Colón, H. Yin, J. Roque, P. Konda, S. Gujar, R.P. Thummel, L. Lilge, C.G. Cameron, S.A. McFarland, *Chem. Rev.* 119 (2019) 797–828.
- [6] S. Swaminathan, J. Haribabu, N. Balakrishnan, P. Vasanthakumar, R. Karvembu, *Coord. Chem. Rev.* 459 (2022), 214403.
- [7] M. Bashir, I.A. Mantoo, F. Arjmand, S. Tabassum, I. Yousuf, *Coord. Chem. Rev.* 487 (2023), 215169.
- [8] A. Romero, T. Campos-Malpartida, C. Lidrissi, M. Saoud, M. Serrano-Ruiz, M. Peruzzini, J.A. Garrido-Cárdenas, F. García-Maroto, *Inorg. Chem.* 45 (2006) 1289–1298.
- [9] B. Sierra-Martin, M. Serrano-Ruiz, F. Scalambra, A. Fernandez-Barbero, A. Romero, *Polymers* 11 (2019) 1–8.

- [10] T. Makovec, *Radiol. Oncol.* 53 (2019) 148–158.
- [11] L. Biancalana, M. Gruchala, L.K. Batchelor, A. Blauz, A. Monti, G. Pampaloni, B. Rychlik, P.J. Dyson, F. Marchetti, *Eur. J. Inorg. Chem.* (2020) 1061–1072.
- [12] T.S. Morais, A. Valente, A.I. Tomaz, F. Marques, M.H. Garcia, *Future Med. Chem.* 8 (2016) 527–544.
- [13] A. Valente, T.S. Morais, R.G. Teixeira, C.P. Matos, A.I. Tomaz, M. Helena Garcia, *Synthetic Inorganic Chemistry: New Perspectives*, 2021, pp. 223–276.
- [14] L. Côte-Real, R.G. Teixeira, P. Gfiro, E. Comsa, A. Moreno, R. Nasr, H. Baubichon-Cortay, F. Avecilla, F. Marques, M.P. Robalo, P. Falson, A. Valente, *Inorg. Chem.* 57 (2018) 4629–4639.
- [15] R.G. Teixeira, A.R. Brás, L. Côte-Real, R. Tatikonda, A. Sanches, M.P. Robalo, F. Avecilla, T. Moreira, M.H. Garcia, M. Haukka, A. Preto, A. Valente, *Eur. J. Med. Chem.* 143 (2018) 503–514.
- [16] R.G. Teixeira, I.C. Salaroglio, N.F.B. Oliveira, J.G.N. Sequeira, X. Fontrodona, I. Romero, M. Machuqueiro, A.I. Tomaz, M.H. Garcia, C. Riganti, A. Valente, *J. Med. Chem.* 66 (2023) 14080–14094.
- [17] R.G. Teixeira, D.C. Belisario, X. Fontrodona, I. Romero, A.I. Tomaz, M.H. Garcia, C. Riganti, A. Valente, *Inorg. Chem. Front.* 8 (2021) 1983–1996.
- [18] A. Isabel, T. Jakusch, T.S. Morais, F. Marques, R.F.M. De Almeida, F. Mendes, É. A. Enyedy, I. Santos, J. Costa, T. Kiss, M.H. Garcia, *J. Inorg. Biochem.* 117 (2012) 261–269.
- [19] V. Moreno, M. Font-bardia, T. Calvet, J. Lorenzo, F.X. Avilés, M.H. Garcia, T. S. Morais, A. Valente, M.P. Robalo, *J. Inorg. Biochem.* 105 (2011) 241–249.
- [20] T.S. Morais, F.C. Santos, T.F. Jorge, L. Côte-Real, P.J.A. Madeira, F. Marques, M. P. Robalo, A. Matos, I. Santos, M.H. Garcia, *J. Inorg. Biochem.* 130 (2014) 1–14.
- [21] L. Gano, T. Pinheiro, A.P. Matos, F. Tortosa, T.F. Jorge, M.S. Gonçalves, M. Martins, T.S. Morais, A. Valente, A.I. Tomaz, M.H. Garcia, F. Marques, *Anti Cancer Agents Med. Chem.* 19 (2019) 1–14.
- [22] L. Côte-Real, B. Karas, P. Gfiro, A. Moreno, F. Avecilla, F. Marques, B.T. Buckley, K.R. Cooper, C. Doherty, P. Falson, M.H. Garcia, A. Valente, *Eur. J. Med. Chem.* 163 (2019) 853–863.
- [23] M.I. Bruce, N.J. Windsor, *Aust. J. Chem.* 30 (1977) 1601–1604.
- [24] T.S. Morais, F.C. Santos, T.F. Jorge, L. Côte-Real, P.J.A. Madeira, F. Marques, M. P. Robalo, A. Matos, I. Santos, M.H. Garcia, *J. Inorg. Biochem.* 130 (2014) 1–14.
- [25] L. Côte-real, M.P. Robalo, F. Marques, G. Nogueira, F. Avecilla, T.J.L. Silva, F. C. Santos, A.I. Tomaz, M.H. Garcia, A. Valente, *J. Inorg. Biochem.* (2015) 1–12.
- [26] L. Côte-Real, B. Karas, A.R. Brás, A. Pilon, F. Avecilla, F. Marques, A. Preto, B. T. Buckley, K.R. Cooper, C. Doherty, M. Helena Garcia, A. Valente, *Inorg. Chem.* 58 (2019) 9135–9149.
- [27] L. Zékány, I. Nagypál, in: N.Y.D.L. Leggett (Ed.), *Computational Methods for the Determination of Stability Constants*, Plenum Press, 1985, pp. 291–353.
- [28] M.D. Hall, M.D. Handley, M.M. Gottesman, *Trends Pharmacol. Sci.* 30 (2009) 546–556.
- [29] C. Teixeira-Guedes, A.R. Brás, R.G. Teixeira, A. Valente, A. Preto, *Pharmaceutics* (2022), <https://doi.org/10.3390/pharmaceutics14061293>.
- [30] H.W. Boucher, V.G. Fowler, A. Jezek, K. Outtersson, D.E. Greenberg, Antibiotic resistance in the patient with cancer: escalating challenges and paths forward, *CA A Cancer J. Clin.* 71 (6) (2021) 488–504.
- [31] J. García-Lara, F. Weihs, X. Ma, L. Walker, R.R. Chaudhuri, J. Kasturiarachchi, H. Crossley, R. Golestanian, S.J. Foster, *Proc. Natl. Acad. Sci. U.S.A.* 112 (2015) 15725–15730.
- [32] A. Mouwakeh, A. Kincses, M. Nové, T. Mosolygó, C. Mohácsi-Farkas, G. Kiskó, G. Spengler, *Phyther. Res.* 33 (2019) 1010–1018.
- [33] E.M. Lewandowski, J. Skiba, N.J. Torelli, A. Rajnisz, J. Solecka, K. Kowalski, Y. Chen, *Chem. Commun.* 51 (2015) 6186–6189.
- [34] J.W. Southwell, R. Herman, D.J. Raines, J.E. Clarke, I. Böswald, T. Dreher, S. M. Gutenthaler, N. Schubert, J. Seefeldt, N. Metzler-Nolte, G.H. Thomas, K. S. Wilson, A.K. Duhme-Klair, *Chem. Eur. J.* 29 (10) (2023), e202202536.
- [35] G. Fanali, A. Di Masi, V. Trezza, M. Marino, M. Fasano, P. Ascenzi, *Mol. Aspect. Med.* 33 (2012) 209–290.
- [36] T. Peters, *All about Albumin: Biochemistry, Genetics and Medical Applications*, Academic Press, San Diego, 1996.
- [37] O. Dömötör, É.A. Enyedy, *J. Biol. Inorg. Chem.* 24 (2019) 703–719.
- [38] O. Dömötör, C.G. Hartinger, A.K. Bytsek, T. Kiss, B.K. Keppler, É.A. Enyedy, *J. Biol. Inorg. Chem.* 18 (2013) 9–17.
- [39] T.S. Morais, F. Santos, L. Côte-Real, F. Marques, M.P. Robalo, P.J.A. Madeira, M. H. Garcia, *J. Inorg. Biochem.* 122 (2013) 8–17.
- [40] APEX3 v2018 1-0, BRUKER AXS, 2018.
- [41] SAINT V8.38A, Bruker AXS Inc., 2017.
- [42] G.M. Sheldrick, SADABS-2016/2 - Bruker AXS area detector scaling and absorption correction, 2008.
- [43] G.M. Sheldrick, *Acta Crystallogr. Sect. A Found. Crystallogr.* 64 (2008) 112–122.
- [44] É.A. Enyedy, N.V. May, V.F.S. Pape, P. Heffeter, G. Szakács, B.K. Keppler, C. R. Kowol, *Dalton Trans.* 49 (2020) 16887–16902.
- [45] J.R. Lakowicz, *Principles of Fluorescence Spectroscopy*, 3rd Principles of Fluorescence Spectroscopy, third ed., Springer, New York, USA, 2006, 2006.
- [46] M. Pesic, J.Z. Markovic, D. Jankovic, S. Kanazir, I.D. Markovic, L. Rakic, S. Ruzdijic, *J. Chemother.* 18 (2006) 66–73.
- [47] A. Podolski-Renić, M. Jadranić, T. Stanković, J. Banković, S. Stojković, M. Chiourea, I. Aljancić, V. Vajs, V. Tešević, S. Ruždijić, S. Gagos, N. Tanić, M. Pešić, *Cancer Chemother. Pharmacol.* 72 (2013) 683–697.
- [48] S. Long, D.I.S.P. Resende, A. Kijjoa, A.M.S. Silva, R. Fernandes, C.P.R. Xavier, M. H. Vasconcelos, E. Sousa, M.M.M. Pinto, *Molecules* 24 (2019) 1–17.
- [49] GraphPad Prism Version 7.00 for Windows, Graph Pad Software: La Jolla, CA, USA, 2018. <http://www.graphpad.com>. accessed n 01.06.2023.
- [50] H. Branco, J. Oliveira, C. Antunes, L.L. Santos, M.H. Vasconcelos, C.P.R. Xavier, *Int. J. Mol. Sci.* 23 (2022) 1–16.
- [51] C.P.R. Xavier, I. Castro, H.R. Caires, D. Ferreira, B. Cavadas, L. Pereira, L.L. Santos, M.J. Oliveira, M.H. Vasconcelos, *Cancer Lett.* 501 (2021) 210–223.
- [52] P. Skehan, R. Storeng, D. Scudiero, A. Monks, J. McMahon, D. Vistica, J.T. Warren, H. Bokesch, S. Kenney, M.R. Boyd, *J. Natl. Cancer Inst.* 82 (1990) 1107–1112.
- [53] V. Vichai, K. Kirtikara, *Nat. Protoc.* 1 (2006) 1112–1116.
- [54] A. Teixeira, D.C. Dacunha, L. Barros, H.R. Caires, C.P.R. Xavier, I.C.F.R. Ferreira, M.H. Vasconcelos, *Food Funct.* 10 (2019) 3188–3197.